Tectonic interpretation in the Modi Khola valley, central Nepal using zirconium-in-rutile thermometry

Todd Reitz

GEOL 394

11/26/14

Aaron Martin

Sarah Penniston-Dorland

Philip Piccoli

ABSTRACT

Tectonic interpretations in the Modi Khola valley, central Nepal were made using estimates of pressures and temperatures by both Martin et al. (2010) and Corrie and Kohn (2011). A kilometer north of the Main Central thrust, both teams inferred the presence of the Bhanuwa fault. However, Martin et al. (2010) interpreted the Bhanuwa fault to be a normal fault, while Corrie and Kohn (2011) interpreted the Bhanuwa fault to be a thrust. Rock samples, the same ones as those studied by Martin et al. (2010), are analyzed with the petrographic microscope for required mineral assemblage in zirconium-in-rutile thermometry. The zirconium-in-rutile thermometer calibration proposed by Tomkins et al. (2007) is used to estimate temperatures based on the cation exchange between zircon and rutile. If calculated temperatures are interpreted as closure temperatures, they can be used along with other values in the expression for closure temperatures derived by Dodson (1973). This expression can be solved to calculate for cooling rates. Footwall samples gave a range of temperatures from 641-674 °C, corresponding to cooling rates of 13-40 K/m.y. Hanging wall samples gave a range of temperatures from 598-649, corresponding to cooling rates of 3-15 K/m.y. The faster cooling rate of footwall relative to hanging wall suggests faster exhumation rate for the footwall. A faster exhumation of the footwall is a normal fault. Therefore I conclude that the Bhanuwa fault is a normal fault and calls into question some details of some tectonic evolution models.

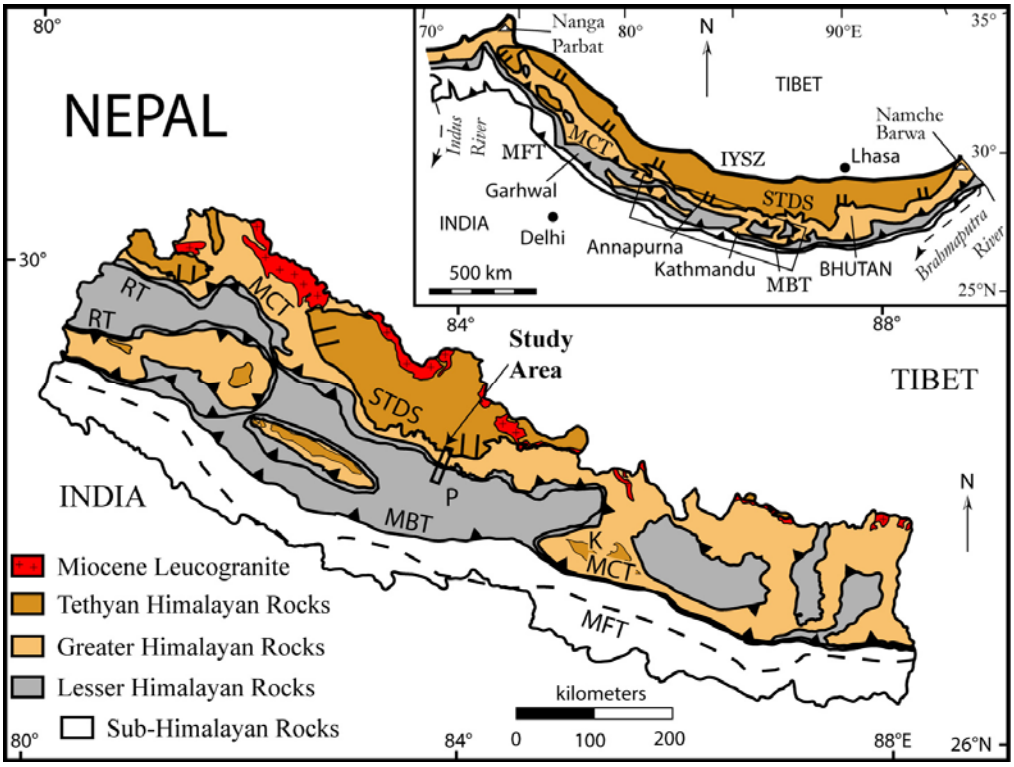

Figure 1: Map of Nepal from Amatya and Jnawali (1994). Himalayan Orogen inset from Sorkhabi and Macfarlane (1999).

INTRODUCTION

Himalayan tectonics, particularly in the Modi Khola valley, central Nepal, have been studied by Martin et al. (2010) as well as Corrie and Kohn (2011). Both teams used similar thermobarometric methods to estimate temperatures and pressures. Concentrating on an area located approximately 1km north of the Main Central thrust, each group has interpreted their data of this specific area to contain a fault, named the Bhanuwa fault. Intriguingly, the two teams did not achieve similar pressure and temperature estimates across the fault. These differences of estimates led too different interpretations of the fault. Martin et al. (2010) interpreted this fault to be a normal fault based on three lines of evidence. Frist,

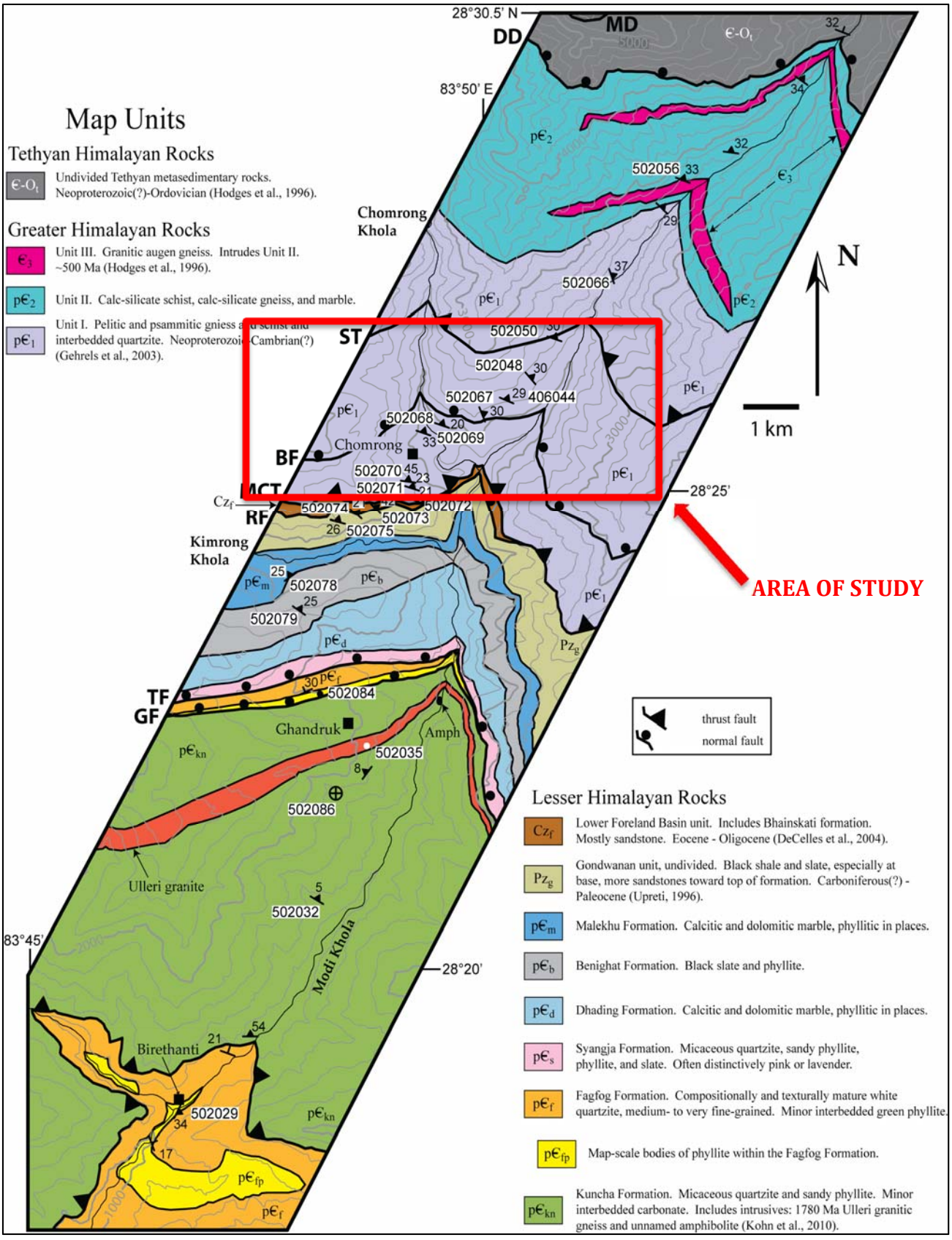

Figure 2: Map of Modi Khola valley, central Nepal from Martin et al. (2010)

there was a 4kbar pressure difference across the fault. Secondly, the footwall cooled more rapidly than the hanging wall, indicated by the footwall containing a shorter retrograde diffusion profile in garnet compared to the hanging wall. Third, samples collected from the hanging wall contained the aluminosilicate kyanite, but samples on the footwall did not contain an aluminosilicate. Conversely, in Corrie and Kohn (2011) their estimates for pressure and temperate did not support Martin et al. (2010) interpretation. The data does not indicate a 4kbar pressure difference, what is shown is very little change in pressure across the fault. However, the data displays an 85°C temperature difference. It is also suggested this temperature increase could account for the longer retrograde diffusion profiles in the hanging wall compared to footwall. Therefore, Corrie and Kohn (2011) reinterpreted the fault to be the Bhanuwa thrust. These discrepancies have implications for the tectonic interpretation of the region. In order to address this problem, the zirconium-in-rutile thermometer method of Tomkins et al. (2007) will be used. Furthermore, the temperatures can be interpreted as closure temperatures and can be used in Dodson (1973) equation for the weighted average of the closure temperatures of a geochronological system. With given and calculated variables associated with this equation, it can be solved to calculate cooling rate.

GEOLOGIC SETTING

Many millions of years ago, the slow, northward moving Indian Tectonic plate collided with the Eurasian plate. The collision caused uplift, and led to the formation of a mountain range. This newly developed mountain range is known today as the Himalayas. Figure 1 shows a generalized geologic map of this mountain range and the contact of the Greater Himalayan, Lesser Himalayan and Tethyan rock formations.

The area of study lies in the area noted in Figure 2, a geologic map of the Modi Khola valley, central Nepal. The study area is located in the Greater Himalayan rock formation. This rock formation can be further subdivided into 3 separate units. A pelitic and psammitic unit with interbedded quartzite, Unit I (Gehrels et al. 2003). Calcareous unit, Unit II, with intrusions of a felsic gneiss, Unit III (Hodges et al. 1996). The structural top of the units is the South Tibetan detachment system (STDS in figures) and the structural base the Main Central thrust (MCT in figures). The South Tibetan detachment system is a series of gently north-dipping normal faults with varying amounts of slip. It is the boundary between overlying Tethyan sedimentary rocks and underlying Greater Himalayan metamorphic rocks (Burchfiel et al. 1992). The Main Central thrust is a broad ductile shear zone and is the boundary between the overlying Greater Himalayan rocks and the underlying Lesser Himalayan rocks, containing at least 160km of slip (Pearson 2002). The area I will be focusing on is the Bhanuwa Fault (BF in figures). This fault is within the Unit I of the Greater Himalayan rocks. Although this fault has not been observed in the field, knowledge of the surrounding faults and foliations helps the interpretation of the presence of a fault dipping 35° to the northeast.

The topographic features of this map also show where the Modi Khola river is located as it runs from north to south slicing through the various rock formations. The samples I have used were collected by Martin et al. (2010) and are shown with strike and dip symbols throughout the cross-section.

BACKGROUND

Martin et al. (2010) calculated temperature and pressure estimates of the Greater and Lesser Himalayan rocks in the Modi Khola valley, central Nepal using thermobarometry. For

their thermobarometric analyses, a garnet-biotite thermometer was used. This is a cation exchange thermometer, where Fe^{2+} exchanges with Mg^{2+} between the minerals, with an uncertainty of ± 35°C. A garnet-muscovite-quartz-biotite-plagioclase barometer, with an uncertainty of 1 kbar, was used. The barometer estimates pressures based on the equilibrium of biotite + plagioclase feldspar = garnet + muscovite + quartz. Across the boundary of the Bhanuwa fault their data indicates a 4 kbar pressure difference, shown by Figure 3. This pressure difference led to the interpretation of a normal fault.

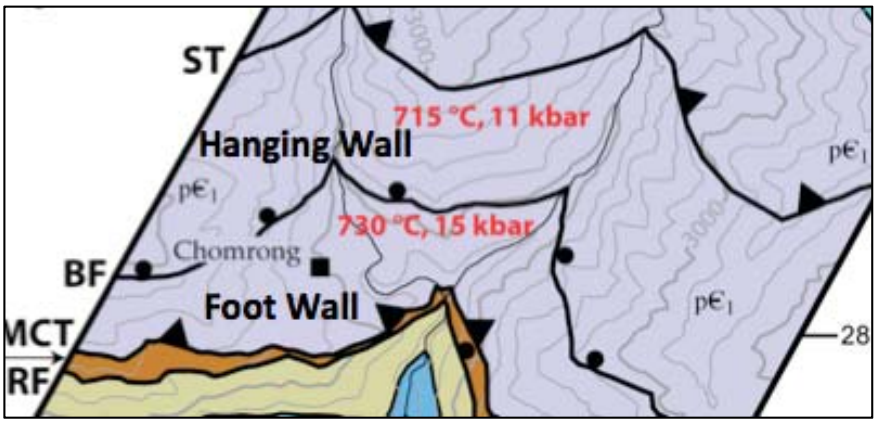

Figure 4: Map from Martin et al (2010). Focused in on the Bhanuwa Fault with pressure and Temperature estimates from Martin et al. (2010)

Conversely, Corrie and Kohn et al. (2011) also calculated temperature and pressure estimates of the Greater and Lesser Himalayan rocks in the Modi Khola valley, central Nepal using thermobarometry. They also used a garnet–biotite thermometer and a garnet-muscovite-quartz-biotite-plagioclase barometer for their thermobarometric analyses. However, a different calibration for their thermometer and barometer were used, but contained similar uncertainties. Corrie and Kohn (2011) also recognized the Bhanuwa fault, but differently from Martin et al. (2010) they found an 85°C temperature difference across the boundary. This temperature difference, shown by Figure 4, led to the interpretation of the fault to be a thrust.

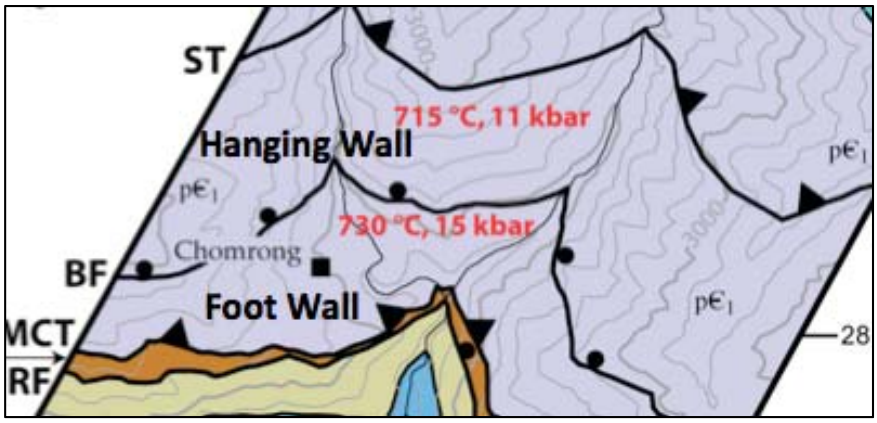

Figure 3: Map from Martin et al (2010). Focused in on the Bhanuwa Fault with pressure and Temperature estimates from Martin et al. (2010)

The conflicting analyses of the fault are important to the geologic community because they affect the interpretation of the tectonic evolution of the area. Martin et al. (2010) and Corrie and Kohn (2011) both provide models of their interpretations of this area. In Martin et al. (2010), they suggest a model of a normal fault in between two thrusts. While, in the Corrie and Kohn (2011) model it suggest a progression of thrust sheets getting younger towards the foreland. These differences effect the interpretation of the overall tectonic evolution of this area. My data can help further suggest one of their models.

HYPOTHESIS

Cooling rate calculations by use of zirconium-in-rutile thermometer estimates are consistent with one side of the Bhanuwa fault cooling faster than the other.

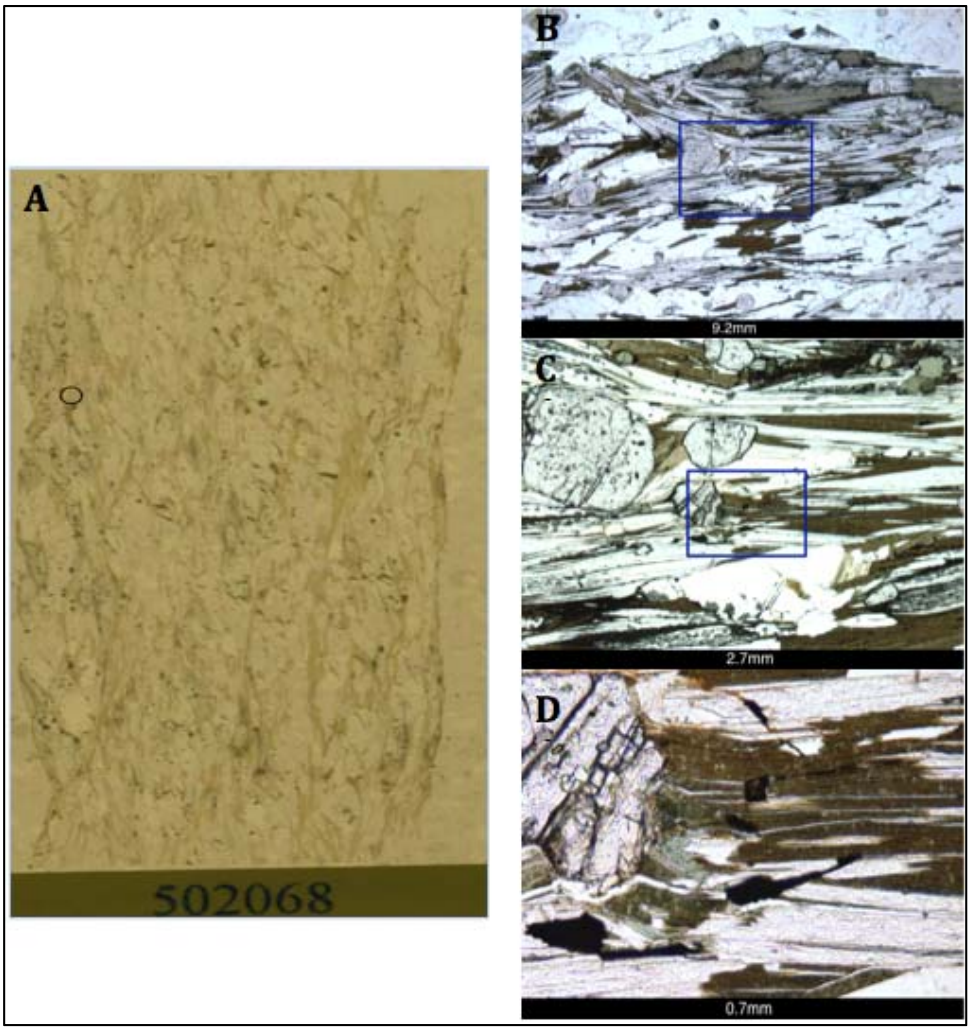

Figure 6: A) rutile location on thin section map B) 1.5x C) 5x D) 20x magnification

EXPERIMENTAL METHODS

Dr. Martin provided thin sections for this study. Thin sections were studied with a petrographic microscope. The goal was to identify the minerals in thin sections. The proper mineral assemblage for the exchange of cations in the zirconium-in-rutile thermometer is needed: quartz + zircon + rutile. The minerals quartz and zircon were likely originally deposited as sediments whereas the rutile likely formed as a result of metamorphism. Once all of the required minerals were located, more importance was placed upon examining the thin section for additional rutile grains. Grains were identified for subsequent analysis by using the electron probe microanalyzer (EPMA). The locations of the grains were then documented at various magnifications as well as on an enlarged thin section map. Beginning with the thin section map, you can locate the specific rutile grain you wish to analyze. When the area is located, progression from 1.5x, to 5x and finally 20x magnification is used to help supplement the search. This process is show by Figure 5.

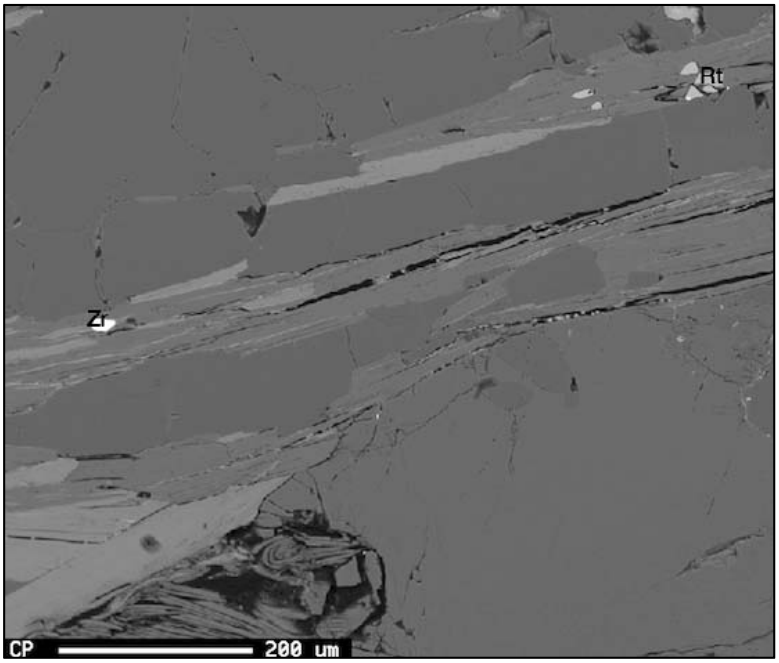

Figure 5: A Back scattered electron image from the EPMA shows a rutile (Rt) grain in close proximity to a grain of zircon (Zr).

ELECTRON PROBE MICROANALYZER

The JEOL JXA 8900R electron probe microanalyzer was used for this study. The electron probe microanalyzer bombards the thin section with a beam of electrons causing the emission of characteristic wavelengths of elements. These wavelengths are reflected into a detector to allow for the analysis of elemental concentrations of minerals.

The following operating conditions were used: 3 μm beam diameter, 20 kV acceleration voltage, 120 nA current, counting times of 300 seconds on peak and 150 seconds on each side of background. Zirconium was measured using the PETH detector, a wavelength dispersive spectrometer. Concentrations measured include Zr, Ti, V, Mn, Al, Cr, Fe, Si, Nb and Ta.

Uncertainty

The EPMA data are reported as zirconium oxide (ZrO_2) weight percent, they must be converted into parts per million (ppm) of zirconium. To accomplish this, start with the zirconium oxide weight percent and multiply by 10000. Now the ZrO_2 is in ppm, however ppm zirconium (Zr) is required for the thermometer. Converting to Zr ppm the molecular weight ratio of Zr to ZrO_2 is needed. The molecular weight of Zr is 91.224 and the molecular weight of oxygen (O) is 15.999. Multiply the molecular weight of O by 2 because there are 2 atoms of O, and add together with Zr to get the total molecular weight of 123.222 for ZrO_2. Take the molecular weight of Zr and divide by ZrO_2 to find the ratio of Zr to ZrO2. This ratio is calculated to 0.7403 or 74.03%. Multiplying this ratio by ppm ZrO_2 gives the Zr concentration in ppm, the value can finally be used in the thermometer.

ZIRCONIUM-IN-RUTILE THERMOMETER

As Tomkins et al. (2007) states in their paper, a potentially powerful thermometer is recognized when rutile is found along with zircon and quartz because the solubility of ZrO_2 has a large dependence on temperature. I have identified the appropriate assemblage (zircon, rutile and quartz) in the samples used in this study. This thermometer works on the basis of zirconium (Zr^{4+}) substitutes more readily in for titanium (Ti^{4+}) in rutile with increasing temperatures. Thus, a higher temperature would allow for a higher zirconium concentration to be accommodated in the rutile grain. Due to the zirconium ion being larger than the titanium ion, Tomkins et al. expected this volume change could cause a decrease in zirconium concentrations with increasing pressures. They examined this possible secondary pressure effect with a piston cylinder set at 10, 20 and 30 kbar along with a 1 atm furnace on the ZrO_2-TiO_2-SiO_2 system. Their experiment showed the solubility of ZrO_2 in rutile, while in the presence of quartz and zircon, reversed at each given pressure value (Tomkins et al. 2007). Thus, allowing them to derive the equations based on the equilibrium of zircon=quartz+ZrO_2 (in rutile). However, the assumptions of rutile growing in the presence of zircon and quartz as well as the rutile not re-equilibrating during cooling must be made.

The calibration I will be using is in the α-quartz field due to estimates from other works (Martin et al. 2010, Corrie and Kohn 2011) plotting in the α-quartz field on a pressure-temperature diagram.

$$T(°C)=\frac{83.9+0.410P}{0.1428-R\ln\phi}-273 \qquad \text{(Equation 1)}$$

Where P is pressure in kbar, R is the gas constant (0.0083144 kJ/K), and ϕ is the Zr concentration in ppm.

Uncertainty

All concentration measurements have uncertainties associated with them. Uncertainties associated with the electron probe microanalyzer for major elements, are estimated from a modified version of the equation $1\sigma = \left(\frac{\sqrt{N}}{N}\right) 100\%$, where N is the number of counts at peak position (above the background). A modified version is needed since trace elements are being measured and the counting of the background becomes more important. These relative uncertainties are given as percent, but they can be converted to absolute uncertainties as ppm.

An example of this is a grain with a Zr concentration of 120 ppm with a 15% uncertainty at the 1σ level. To convert this to absolute uncertainty, 120 ppm*0.15= 18ppm at 1σ. At the 2σ level, 18*2=36 ppm. This is written as 120±36 ppm. Now we have the uncertainty on the concentration of Zr, and this uncertainty can further be used to get a range of temperatures from the zirconium-in-rutile thermometer. For this example, given the α-quartz equation at 12kbar, this will give a temperature range of 565-608°C. This process will then be repeated for each spot on each grain.

COOLING RATE

Dodson (1973) defines closure temperature as the temperature at the time corresponding to its apparent age. In his paper he derives an expression for the weighted average of the closure temperatures of a geochronological system. The following assumptions must be made before this equation can be used:

(1) The mineral of interest has a homogeneous distribution of the parent and daughter nuclides at the peak thermal condition
(2) It is surrounded by sufficiently large mass of fast diffusing matrix so that they composition of the matrix remains effectively homogenous and fixed
(3) The surface composition of the mineral is in equilibrium with the matrix during cooling and changes uniformly with time
(4) The cooling is monotonic
(5) The mineral is isotropic with respect to diffusion
(6) The mineral has suffered a complete "memory loss" of its concentration of radiogenic daughter product established at T_0. (Dodson 1973)

$$\frac{E}{RT_c} = \ln(-(ART_c{}^2 D_0)/(Ea^2\left(\frac{dT}{dt}\right)) \qquad \text{(Equation 2)}$$

Where E is the activation energy, R is the gas constant, T_c is the closure temperature, A is the geometric factor ($A=e^G$), D_0 is the pre-exponential factor in the Arrhenian expression of diffusion coefficient, a is the radius of the grain and (dT/dt) is the cooling rate. Values determined from Cherniak et al. (2007) for E and D_0, given at 170±30 kJ/mol for E and $9.8E^{-11}$ cm^2/s for D_0. It was concluded by Blackburn et al. (2012) 200kJ/mol is the more appropriate value. Values for T_c and a are my estimated temperatures by zirconium-in-rutile thermometer and radiuses determined from photomicrograph images. For A, the G for sphere is given as 4.0066 from Ganguly and Massimilano (2009). Applying these values and my estimated values for T_c (K) and estimated radius measurements, a (cm), the equation can be solved for the cooling rate (dT/dt).

$$\frac{dT}{dt} = -\frac{ART_C^2 D_0}{Ea^2} * 1/e^{E/RT_c} \qquad \text{(Equation 3)}$$

Estimates are obtained in Kelvin/second (K/s) and must be converted to Kelvin/million years (K/m.y). Multiplying estimates by $3.2E^{13}$ seconds (calculated by 60seconds/min*60min/hr.*24hr./day*365day/yr.*1000000yr) in a million years achieves this task.

Cooling rates by themselves are not useful for determining the sense of motion of a fault, but the relative cooling rates of one side of the fault to the other side are useful. Assume the faster cooling rate is due to a faster exhumation rate and the transformation from cooling rate to exhumation rate was the same for both the hanging wall and footwall. The assumptions then allow for an interpretation of the sense of motion of the fault to be determined.

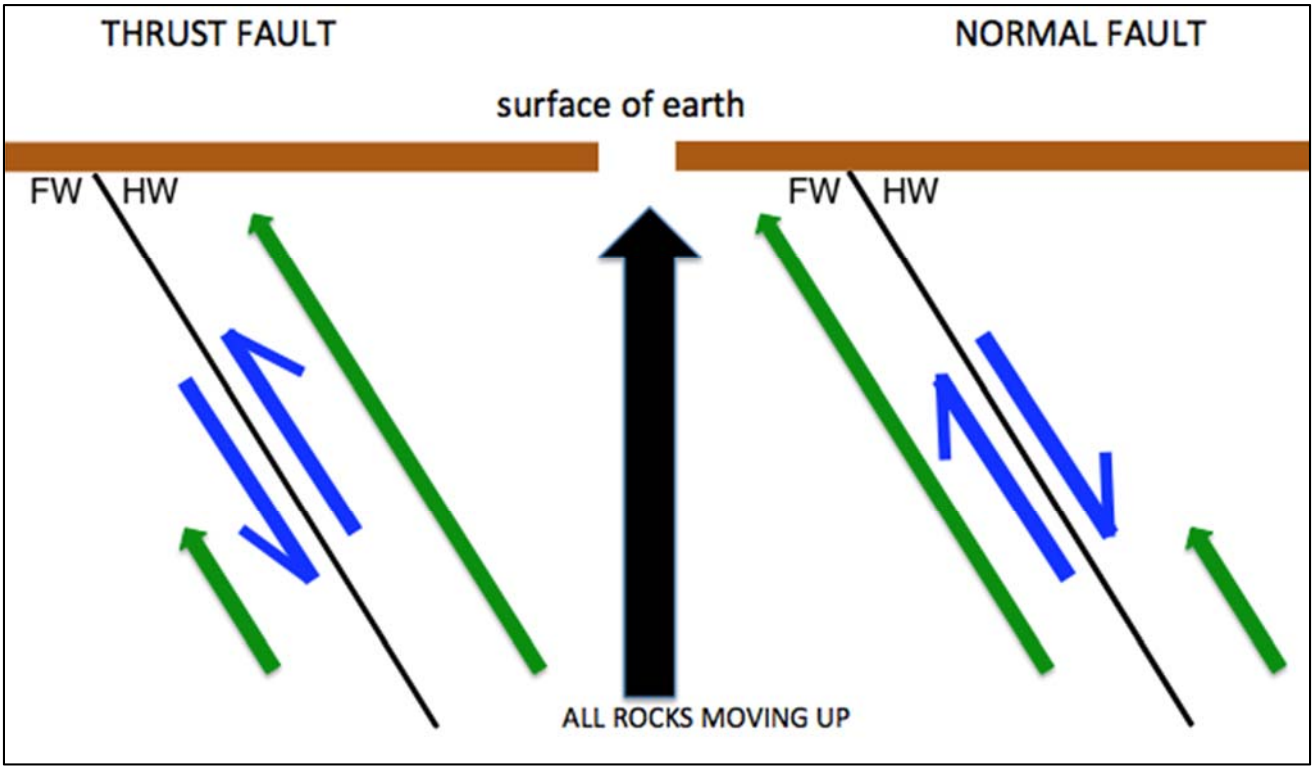

Figure 7: Diagram showing motion of a fault using cooling rates. BLUE shows relative motion across the fault. GREEN shows motion relative to surface of earth.

Figure 7 shows how to determine sense of motion of a fault based on the relative cooling rates on either side of the fault. The blue arrows are showing what typical fault motions look like for a normal fault, with the footwall moving up relative to the hanging wall, and a thrust fault, with the hanging wall moving up relative to the footwall. With all rocks moving upwards towards the surface of the earth, exhumation rates can be added in. The green arrows show the exhumation rates or the motion relative to the surface of the earth, with the longer green arrows correlating to a faster exhumation rate. These green arrows show, while both sides are moving up, the side with the faster exhumation rate is moving up more quickly than the other side. Thus, a thrust fault will have a greater exhumation rate on the hanging wall relative to the footwall. Conversely, a normal fault will have a greater exhumation rate on the footwall relative to the hanging wall.

Uncertainty

While all the variables associated with equation 3 contain uncertainty in their

measurement for the calculation of the true magnitude of the cooling rate. For the purposes of this study in terms of relative cooling rates of the hanging wall to footwall, most of these uncertainties cancel out. The analytical uncertainties from the electron probe microanalyzer and the uncertainty of grain size, more importantly its radius, does not cancel out. Before, measurements are estimated, the assumption of the mineral following a similar structure in 3-D to that of the 2-D view cut shown in thin section must be made.

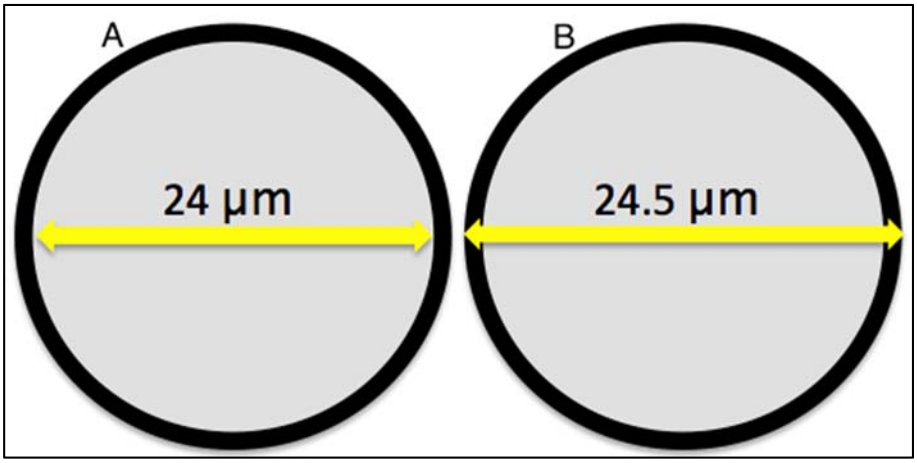

Figure 8: A) Shows the small diameter measurement. B) Shows the large diameter measurement.

Uncertainty of radius measurements can be estimated by measuring the inside line of the grains edge to the other inside of the grains edge and measuring the outside line of the grains edge to the outside line of the grains edge. This will give me a small measurement of diameter and a large measurement of the diameter. Figure 8 shows this process. Dividing the numbers by 2 gives the radius. For the rutile used in the analysis there is ~.3 micron difference in measurement of the radius. Pairing the small radius measurement with the +2σ upper bound of the temperature yields the largest value for cooling rate. While, the smallest value of cooling rate comes from combination of the large radius measurement and the -2σ lower bound of the temperature. A grain with a radius of 12µm and a temperature of 900K, will generate a cooling rate of 10 ± 3.5 K/m.y.

small radius (µm)	plus 2σ temp. (K)	high cooling rate (K/m.y)
11.7	910	14
large radius	minus 2σ temp. (K)	low cooling rate (K/m.y)
12.3	890	7

Table 1: Cooling rate uncertainty calculation example.

Possible Limitation

Taylor-Jones and Powell (2014) provide new evidence for interpretation of temperature estimates calculated by a zirconium-in-rutile thermometer. Analysis of diffusion data, specifically zirconium in rutile diffusion, suggests the thermometer will not yield the high temperatures usually achieved in high grade metamorphic rocks. Their observations can be attributed to a high diffusive closure of silicon (Si) in rutile, slow grain boundary diffusion and problematic zircon nucleation. Ultimately, they imply use of a zirconium-in-rutile thermometer to estimate cooling rates will not be useful. If correct, this is a potential limitation on the conclusions of this project.

EXPERIMENTAL DATA

		TEMPERATURE (°C)		RADIUS (µm)	COOLING RATE (K/m.y)	
SAMPLE	Grain #	Martin pressures ±2σ	C+K pressures ±2σ	±2σ	Martin pressures ±2σ	C+K pressures ±2σ
Footwall						
502068	4	665 ± 9	652 ± 9	13 ± 0.4	28 ± 9	19 ± 6
502069	4	664 ± 10	651 ± 10	12 ± 0.2	30 ± 10	21 ± 7
Hanging wall						
502067	2A	611 ± 13	618 ± 13	11 ± 0.3	7 ± 4	10 ± 4
502067	2B	630 ± 11	638 ± 11	14 ± 0.2	8 ± 3	11 ± 4

Table 2: Table 2: Data analysis. Column with Martin pressures refers to the use of Martin et al. (2010) pressures. Columns with C+K pressures refer to the use of Corrie and Kohn (2011) pressures.

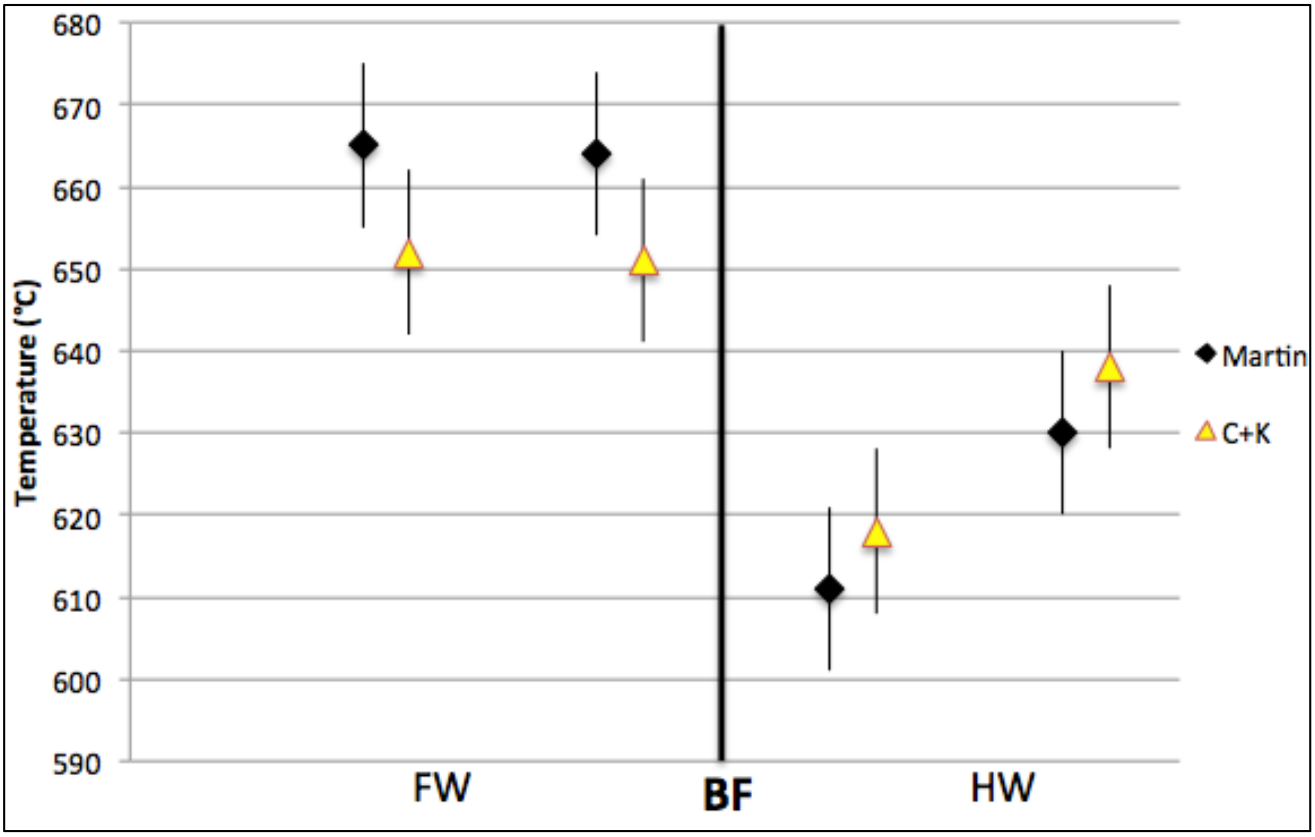

Figure 9: Graph of temperature estimates across the Bhanuwa fault (BF). Samples from the footwall (FW) are on the left and samples from hanging wall (HW) are on the right. Black rhombuses indicate pressures used from Martin et al. (2010). Yellow triangles indicate pressures used from Corrie and Kohn (2011).

Temperature estimates across the Bhanuwa fault in the Greater Himalayan rocks are show in Figure 9. The data on the left side are from the footwall and the data on the right side from the hanging wall. The Martin data, shown with the black rhombuses, uses the pressure estimates in the hanging wall and footwall from Martin et al. (2010), and the Corrie and Kohn data, shown with the yellow triangles, using the hanging wall and footwall pressure estimates

from Corrie and Kohn (2011). These pressures were used in Equation 1 along with Zr concentrations analyzed to estimate temperature values.

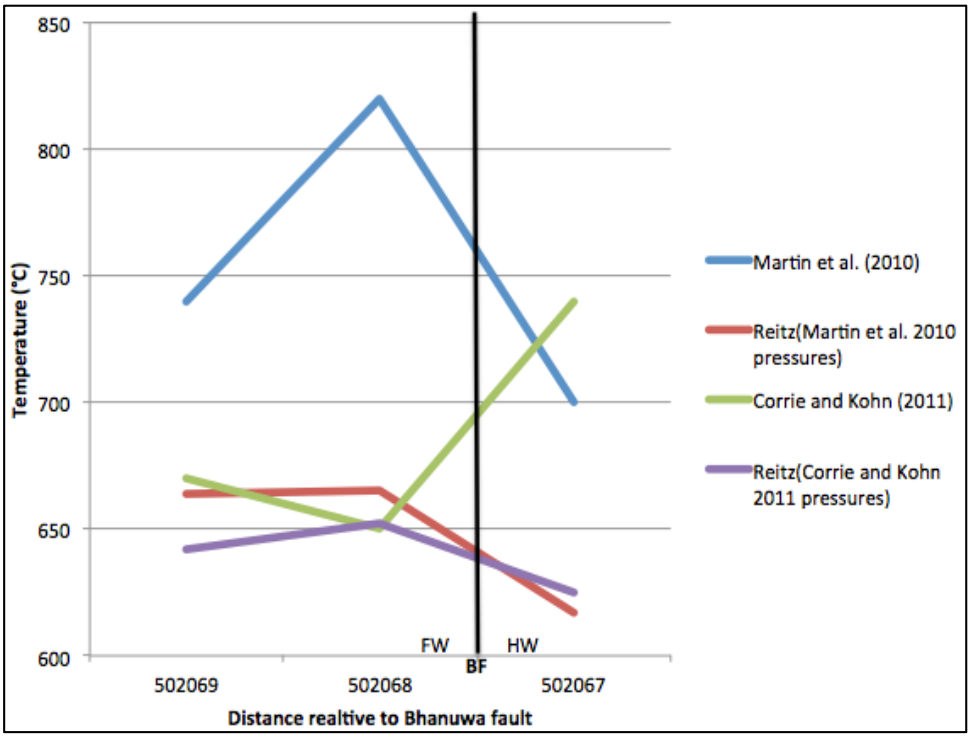

Figure 10: Comparison of temperature estimates across Bhanuwa fault. Martin et al. (2010) and Reitz used thin sections labeled on x-axis. Similar thin sections were located in Corrie and Kohn (2011) by distance away from fault. AS01-15c for 502069, AS01-33b for 502068, and AS01-16a for 502067.

After the calculations were completed, temperatures were noticeably lower relative to the other works. Discussing the issue, the conclusion determined the rutile grains found in the Greater Himalayan rocks, are too small to record the peak temperatures. However, if the values are interpreted as closure temperatures, they could input into Equation 3 to approximate the

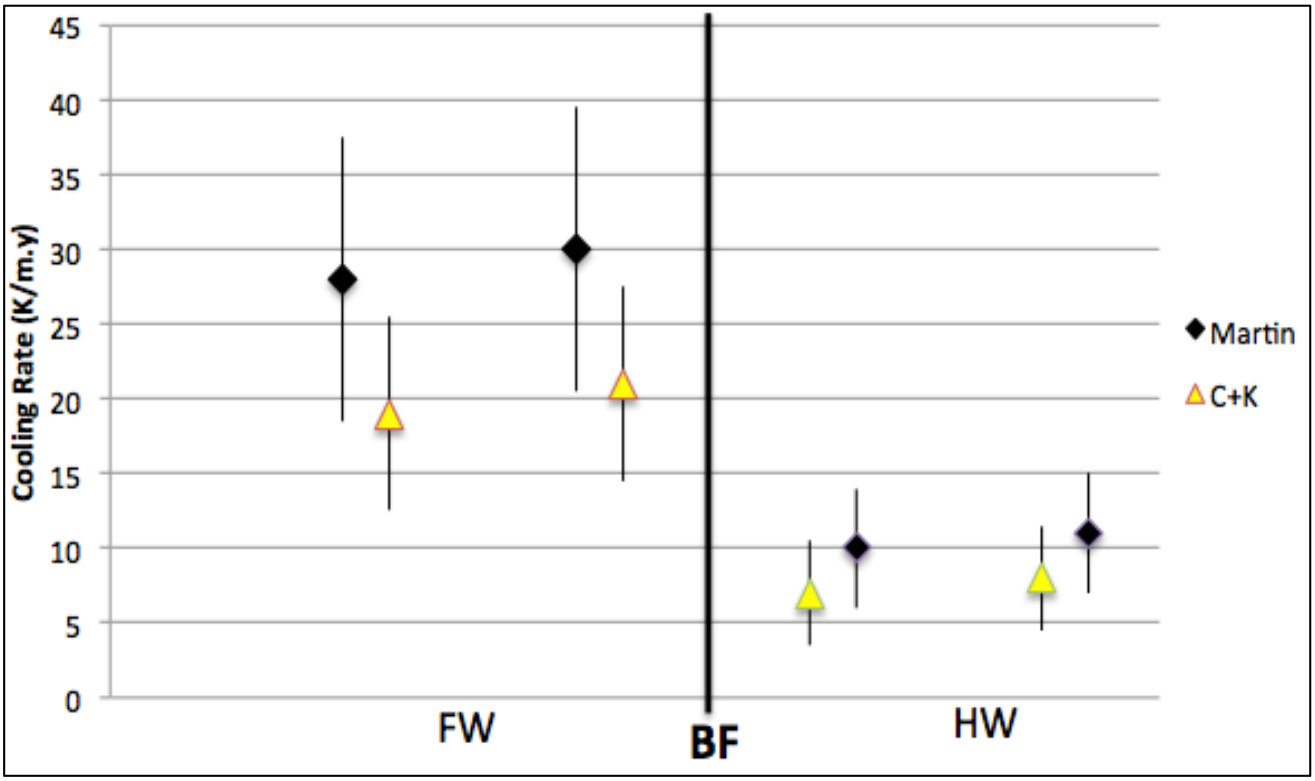

Figure 11: Graph of cooling rate estimates across the Bhanuwa fault (BF). Samples from the footwall (FW) are on the left and samples from hanging wall (HW) are on the right. Black rhombuses indicate pressures used from Martin et al. (2010). Yellow triangles indicate pressures used from Corrie and Kohn (2011).

cooling rate of one side relative to the other.

Cooling rate estimates across the Bhanuwa fault in the Greater Himalayan rocks are shown in Figure 11. The data on the left side are from the footwall and the data on the right side from the footwall. The Martin data, shown with the black rhombuses, uses the pressure estimates in the hanging wall and footwall from Martin et al. (2010), and the Corrie and Kohn data, shown with the yellow triangles, using the hanging wall and footwall pressure estimates from Corrie and Kohn (2011). These pressures, estimated temperatures, estimated grain dimensions and values establish in other papers were used to approximate cooling rates of one side relative to the other.

DISCUSSION

The estimated closure temperatures I calculated are interpreted as being lower than the peak temperatures the rocks experienced. Therefore, the rocks cooled by about 100°C or more before capturing in the Zr concentrations in the rutile grains. To compensate the pressure values for both previous studies were reduced by 2 kbars. The pressure effect of this is very small, if this value was doubled to 4kbars then the effect on temperature would be ~15°C, which in turn only causes the cooling rate to change by ~5K/m.y, with a 12μm and 900K rutile. However, this only has a net effect on the absolute value of cooling rate, it does not effect the cooling rate of one side relative to the other.

7 thin sections in total were examined, however only 4 contained the needed mineral assemblage for this study. In addition, of these 4 thin sections analyzed by the electron probe microanalyzer, only 4 grains in total from 3 thin sections were used in the data analysis. These grains were selected because they are biggest and most comparable sizes available. The biggest grains are assumed to be the closest to the center cut of the grain, while similar sizes in grains were needed in order to compare uniform data across the fault. Data both larger (found in sample 502067) and smaller (samples 502050, 502068, and 502069) were unused for not meeting these specified criteria.

Comparing data, by use of the method described by Figure 7 indicates the footwall samples relative to the hanging wall samples cooling at a faster rate. A faster cooling rate in the footwall suggests a faster exhumation rate. Given this interpretation of faster footwall exhumation, or footwall moving up relative to the hanging wall. When the footwall has an upward sense of motion relative to the hanging wall, the fault is interpreted as a normal fault. Thus, it can be concluded the data suggests the Bhanuwa fault is a normal fault. The data helps further suggest the Bhanuwa fault is a normal fault in between thrust, the model proposed by Martin et al. (2010), as opposed to a series of thrust sheets, the model proposed by Corrie and Kohn (2011).

He et al. (2015) modeled the Miocene tectonic evolution of the Himalaya via growth of a duplex in Greater Himalayan rocks. For this model to work, they require multiple thrust faults within Greater Himalayan rocks, and they used the thrusts described by Corrie and Kohn (2011), among others. He et al. made no allowance for a normal fault active at this time within Greater Himalayan rocks. Thus my conclusion of a normal fault within Greater Himalayan rocks calls into question the details of the He et al. (2015) model, though not the conceptual basis for it.

Further analysis of zircons found in thin section using a titanium-in-zircon thermometer, such as the one calibrated by Ferry and Watson (2007), is an option for future work on this project. Investigation of the metamorphic components of the zircon and not the detrital zircons will need to be studied. Cathololuminescence imaging of the zircons helps show the rims and

cores of the zircon grain. The titanium-in-zircon thermometer would be used upon the metamorphic rims identified by these images. Additionally, the rims would also need to be dated to see if they grew during the Miocene epoch. In turn, this new data could be compared back to data collected in this study as well as other works.

REFERENCES

Amatya, K.M. and B.M. Jnawali. Geological map of Nepal. Department of Mines and Geology, Government of Nepal, Scale 1:1,000,000. 1994

Blackburn, T, N Shimizu, S.A. Bowring, B Schoene, K.H. Mahan. "Zirconium in rutile speedometry: New constraints on lower crustal cooling rates and residence temperatures." *Earth and Planetary Science Letters* 317-318 (2012): 231-240. Web 25 April. 2014.

Burchfiel BC, Chen Z, Hodges KV, Liu Y, Royden LH, Deng C, Xu J (1992) The South Tibetan detachment system, Himalayan orogen: Extension contemporaneous with and parallel to short- ening in a collisional mountain belt. *Geological Society of America Special Paper* 269: 1-41

Cherniak, D.J., J Manchester, and E.B. Watson. " Zr and Hf diffusion in rutile." Earth and *Planetary Science Letters* 261 (2007): 267-279. Web. 18 April. 2014

Corrie, S.L., and M.J. Kohn. "Metamorphic history of the central Himalaya, Annapurna region, Napal, and implications for tectonic models." *Geological Society of American Bulletin*. 123. (2011): 1863-1879. Print.

Dodson, Martin H. "Closure Temperature in Cooling Geochronological and Petrological systems." *Contributions to Mineralogy and Petrology,* 40 (1972): 259-274. Web. 18 April. 2014.

Ferry J.M., & Watson, E.B., 2007. New thermodynamic models and revised calibrations for the Ti-in-zircon and Zr-in-rutile thermometers. *Contributions to Mineral Petrology*. 154. 429–437.

Ganguly, J and T. Massimilano. "Closure Temperature, Cooling Age and High Temperature Thermochronology." *Physics and Chemistry of Earth's Interior; Crust, Mantle, Core*. (2009) 89-98. Web. 18 April. 2014.

Gehrels GE, DeCelles PG, Martin A, Ojha TP, Pinhassi G, Upreti BN (2003) Initiation of the Himalayan Orogen as an early Paleozoic thin-skinned thrust belt. *GSA Today* 13(9):4–9.

He, D., Webb, A.A.G., Larson, K., Martin, A.J., and Schmitt, A.K., (2015), Extrusion vs. duplexing models of Himalayan mountain building 3: Duplexing dominates from Oligocene to present: *International Geology Review*, in press, doi:10.1080/00206814.2014.986669.

Hodges KV, Parrish RR, Searle MP (1996) Tectonic evolution of the central Annapurna Range, Nepalese Himalayas. Tectonics 15(6):1264–1291

Martin, A., J. Ganguly, and P. DeCelles. "Metamorphism of Greater and Lesser Himalayan rocks exposed in the Modi Khola valley, central Nepal." *Contributions to Mineralogy and Petrology*. 159. (2010): 203-223. Print.

Pearson, ON. "Structural evolution of the central Nepal fold- thrust belt and regional tectonic and structural significance of the Ramgarh thrust." Ph.D. Dissertation, University of Arizona (2002), 1-231.

Sorkhabi, R.B. and A. Macfarlane. Himalaya and Tibet: mountain roots to mountain tops. In: Macfarlane A, Sorkhabi RB, Quade J (eds) Himalaya and Tibet: mountain roots to mountain tops: special Paper—Geological Society of America. United States, Geological Society of America (GSA), Boulder, CO, pp 1–7. 1999

Taylor-Jones, K. and R. Powell. "Interpreting Zirconium-in-Rutile Thermometric Results ." *Journal of Metamorphic Geology*. doi: 10.1111/jmg.12109

Tomkins, H.S., R Powell, and D.J. Ellis. "The pressure dependence of zirconium-in-rutile thermometer." *Journal of Metamorphic Geology*. 25. (2007): 703-713. Print.

APPENDIX

			TEMPERATURE (°C)				RADIUS (cm)		COOLING RATE (K/m.y.)	
			using		using				using	using
	Grain	Spot	martin pressures	±2σ	C+K pressures	±2σ		±2σ	martin pressures	C+K pressures
Footwall										
502068	1a	2	473	67	463	66	0.00036	0.00002	0.3	0.2
		3	547	31	536	30	0.00036	0.00002	6.8	4.4
		4	480	61	469	60	0.00036	0.00002	0.4	0.3
		5	510	47	499	46	0.00036	0.00002	1.5	1.0
	2	1	594	18	582	18	0.00052	0.00004	17.5	11.5
		2	585	20	573	19	0.00052	0.00004	13.0	8.5
		3	592	18	580	18	0.00052	0.00004	16.2	10.7
		4	600	17	588	17	0.00052	0.00004	21.6	14.3
		5	592	18	580	18	0.00052	0.00004	16.2	10.7
	3	1	607	16	595	15	0.00069	0.00004	15.5	10.3
		2	571	23	559	22	0.00069	0.00004	4.4	2.9
		3	600	17	588	17	0.00069	0.00004	12.3	8.1
	4	1	663	9	650	9	0.00123	0.00002	28.7	19.5
		2	667	9	654	9	0.00123	0.00002	31.6	21.4
502069	1	1	606	17	594	17	0.00060	0.00004	32.7	13.2
	2	1	640	12	628	12	0.00052	0.00004	80.2	54.0
	3	1	600	18	588	18	0.00039	0.00003	38.4	25.4
		2	592	20	581	19	0.00039	0.00003	29.7	19.6
		3	590	20	578	20	0.00039	0.00003	27.1	17.8
	4	1	666	10	653	9	0.00125	0.00004	30.2	20.6
		2	657	10	645	10	0.00133	0.00004	20.5	13.9
		3	663	10	650	10	0.00133	0.00004	24.2	16.4
		4	666	10	654	9	0.00115	0.00002	35.9	24.4
		5	664	10	651	10	0.00133	0.00004	24.8	16.8
		6	666	10	653	10	0.00133	0.00004	26.2	17.8
		7	668	10	655	9	0.00125	0.00004	31.6	21.5
Hanging Wall										
502050	2	2	555	23	562	23	0.00050	0.00002	4.6	6.2
		4	593	15	601	15	0.00050	0.00002	18.3	24.1
	3	1	658	8	666	8	0.00058	0.00002	109.1	141.2
		2	645	10	654	10	0.00058	0.00002	74.0	96.2
502067	1	1	672	7	681	7	0.00262	0.00004	8.1	10.4
		2	677	7	686	7	0.00262	0.00004	9.5	12.3
		3	668	7	676	8	0.00262	0.00004	7.1	9.2
		4	664	8	672	8	0.00262	0.00004	6.4	8.2
		5	657	8	665	8	0.00262	0.00004	5.2	6.7
		6	666	8	675	8	0.00262	0.00004	6.8	8.8
		7	672	7	681	7	0.00262	0.00004	8.2	10.6
		8	669	7	677	8	0.00262	0.00004	7.4	9.5
	2a	1	595	15	603	15	0.00085	0.00004	6.7	8.8
		2	580	17	588	17	0.00085	0.00004	4.0	5.3
		3	622	11	630	11	0.00123	0.00002	7.9	10.3
		4	638	10	646	10	0.00123	0.00002	13.2	17.1
		5	597	14	605	15	0.00123	0.00002	3.4	4.5
		6	606	13	614	13	0.00117	0.00004	5.3	6.9
		7	617	12	626	12	0.00117	0.00004	7.6	9.9
		8	630	10	638	11	0.00117	0.00004	11.4	14.8
	2b	1	624	11	633	11	0.00139	0.00002	6.7	8.8
		2	641	9	649	10	0.00139	0.00002	11.4	14.8
		3	635	10	644	10	0.00139	0.00002	9.5	12.4
		4	618	12	626	12	0.00139	0.00002	5.5	7.1
	2c	1	579	17	587	17	0.00298	0.00008	0.3	0.4
		2	658	8	666	8	0.00298	0.00008	4.1	5.3
		3	665	8	674	8	0.00298	0.00008	5.1	6.6
		4	670	7	679	7	0.00298	0.00008	6.0	7.7
		5	672	7	681	7	0.00298	0.00008	6.3	8.1
		6	672	7	681	7	0.00298	0.00008	6.4	8.2
		7	661	8	670	8	0.00298	0.00008	4.6	6.0
		8	637	10	646	10	0.00298	0.00008	2.2	2.9

EPMA RAW DATA

	ZrO2	TiO2	V2O3	Al2O3	Nb2O5	FeO	SiO2	Cr2O3	MnO	Ta2O5	Total
FW_69_1.1	0.0194	97.1719	0.5869	0.0519	0.4770	0.2929	0.0702	0.0128	0.0000	0.0000	98.6831
FW_69_2.1	0.0307	96.4688	0.5832	0.0701	0.5272	0.3680	0.0890	0.0007	0.0000	0.0000	98.1377
FW_69_3.1	0.0178	96.6752	0.6085	0.0723	0.3172	0.3081	0.0910	0.0088	0.0000	0.0000	98.0990
FW_69_3.2	0.0160	96.1137	0.5993	0.0801	0.3514	0.3300	0.1041	0.0134	0.0163	0.0173	97.6417
FW_69_3.3	0.0154	94.8734	0.5244	0.0713	0.2630	0.3085	0.0784	0.0217	0.0057	0.0072	96.1691
FW_69_4.1	0.0424	96.1876	0.6902	0.0480	1.6048	0.7202	0.0177	0.0924	0.0000	0.0000	99.4033
FW_69_4.2	0.0380	96.6567	0.6478	0.0449	1.3225	0.7025	0.0027	0.0850	0.0000	0.1195	99.6197
FW_69_4.3	0.0407	96.5688	0.6700	0.0461	1.4600	0.6598	0.0145	0.0854	0.0000	0.0286	99.5740
FW_69_4.4	0.0425	96.2573	0.7036	0.0529	1.5169	0.6155	0.0145	0.0859	0.0118	0.0288	99.3298
FW_69_4.5	0.0411	96.1947	0.6829	0.0498	1.6482	0.7061	0.0000	0.1139	0.0033	0.0388	99.4789
FW_69_4.6	0.0421	95.9983	0.6971	0.0472	1.4247	0.6677	0.0147	0.0848	0.0000	0.1969	99.1736
FW_69_4.7	0.0432	95.8188	0.7183	0.0397	1.4656	0.6775	0.0216	0.0727	0.0137	0.1717	99.0429
FW_68_1A.1	0.0000	93.1498	0.3344	0.1558	2.0464	1.3841	0.0496	0.0000	0.0029	0.1532	97.2762
FW_68_1A.2	0.0022	93.9885	0.3170	0.0685	1.9566	1.4403	0.0000	0.0000	0.0000	0.1592	97.9323
FW_68_1A.3	0.0081	93.6934	0.3380	0.0651	1.9044	1.4496	0.0000	0.0000	0.0079	0.1518	97.6183
FW_68_1A.4	0.0025	93.4841	0.3562	0.0675	1.9023	1.4269	0.0000	0.0251	0.0031	0.1774	97.4451
FW_68_1A.5	0.0043	93.8680	0.3445	0.0676	1.8764	1.3916	0.0079	0.0000	0.0040	0.1469	97.7112
FW_68_1B.1	0.0000	93.5914	0.3163	0.0954	1.9079	1.3905	0.0000	0.0000	0.0000	0.1704	97.4719
FW_68_1B.2	0.0000	93.9175	0.3082	0.0805	1.8815	1.4116	0.0000	0.0039	0.0011	0.1498	97.7541
FW_68_4.1	0.0409	95.6850	0.3050	0.0525	0.8295	1.7490	0.0448	0.0000	0.0480	0.0273	98.7820
FW_68_4.2	0.0426	96.6351	0.3391	0.0482	0.8291	1.7001	0.0294	0.0071	0.0345	0.0189	99.6841
FW_68_2.1	0.0163	92.4912	0.2930	0.0332	1.7711	5.0251	0.0372	0.0019	0.2398	0.0311	99.9399
FW_68_2.2	0.0144	96.7857	0.3117	0.2088	0.8733	1.1943	0.0247	0.0000	0.0248	0.0224	99.4601
FW_68_2.3	0.0158	96.8987	0.2609	0.0393	0.7995	1.1485	0.0148	0.0000	0.0055	0.0159	99.1989
FW_68_2.4	0.0178	97.3220	0.2619	0.0360	0.8020	1.1664	0.0265	0.0000	0.0000	0.0294	99.6620
FW_68_2.5	0.0158	97.1061	0.2883	0.0317	0.8383	1.1979	0.0298	0.0000	0.0031	0.0069	99.5179
FW_68_3.1	0.0196	96.8422	0.2756	0.0496	0.7370	1.0558	0.0415	0.0000	0.0029	0.0010	99.0252
FW_68_3.2	0.0116	96.5754	0.2537	0.0386	0.5642	0.9671	0.0366	0.0000	0.0000	0.0001	98.4473
FW_68_3.3	0.0178	96.7322	0.2636	0.0322	0.6345	1.0134	0.0315	0.0000	0.0000	0.0056	98.7308
HW_50_1.1	0.0000	81.8940	0.3606	0.0324	2.2880	1.3110	0.0000	0.0355	0.0100	0.1210	86.0525
HW_50_1.2	0.0000	91.6038	0.3803	0.0367	2.5297	1.5158	0.0000	0.0470	0.0002	0.1678	96.2813
HW_50_1.3	0.0000	14.7024	0.0615	0.0703	0.4084	0.2764	0.0000	0.0000	0.0189	0.0000	15.5379
HW_50_1.4	0.0000	15.6807	0.0595	0.0252	0.4633	0.3315	0.0000	0.0000	0.0474	0.0000	16.6076
HW_50_2.1	0.0000	86.9596	0.2992	3.0293	0.3946	3.1359	2.4107	0.0000	0.0667	0.0059	96.3019
HW_50_2.2	0.0115	94.2383	0.3222	1.2164	0.8860	1.3305	1.2697	0.0164	0.0435	0.0645	99.3990
HW_50_2.3	0.0000	90.1634	0.3222	2.9981	0.8219	1.7468	2.7387	0.0026	0.2033	0.0349	99.0319
HW_50_2.4	0.0202	95.5514	0.3567	0.1528	0.8845	1.7067	0.1304	0.0305	0.0247	0.0348	98.8927
HW_67_1.1	0.0558	96.6045	0.4360	0.0965	1.3603	0.5709	0.3063	0.0975	0.0026	0.1061	99.6365
HW_67_1.2	0.0597	96.4977	0.4610	0.0884	1.3795	0.6127	0.0820	0.1244	0.0000	0.1496	99.4550
HW_67_1.3	0.0531	97.4826	0.4742	0.0823	1.4209	0.6260	0.0661	0.0931	0.0000	0.0985	100.3968
HW_67_1.4	0.0507	97.4725	0.4255	0.0951	1.4032	0.6131	0.0365	0.0994	0.0080	0.0943	100.2983
HW_67_1.5	0.0466	97.2649	0.4328	0.0944	1.3385	0.6072	0.0364	0.1108	0.0028	0.1422	100.0766
HW_67_1.6	0.0521	98.0613	0.4586	0.0930	1.3572	0.6460	0.0408	0.0736	0.0157	0.1252	100.9235
HW_67_1.7	0.0561	97.2537	0.4643	0.0886	1.3934	0.6552	0.0492	0.0835	0.0053	0.1028	100.1521
HW_67_1.8	0.0538	97.1241	0.4681	0.0973	1.3614	0.6200	0.0972	0.0865	0.0000	0.1102	100.0186
HW_67_2C.1	0.0166	98.1063	0.3762	0.0314	0.2874	0.5338	0.0407	0.0237	0.0000	0.0000	99.4161
HW_67_2C.2	0.0472	97.3031	0.4366	0.0387	0.8441	0.5271	0.0171	0.0261	0.0000	0.0570	99.2970
HW_67_2C.3	0.0514	97.2061	0.4750	0.0446	1.0700	0.5567	0.0197	0.0566	0.0000	0.0732	99.5533
HW_67_2C.4	0.0548	96.8132	0.4895	0.0813	1.1608	0.5940	0.0025	0.0534	0.0000	0.1408	99.3903
HW_67_2C.5	0.0560	96.6314	0.4736	0.0820	1.1548	0.6042	0.0096	0.0415	0.0088	0.1247	99.1866
HW_67_2C.6	0.0562	96.9258	0.4775	0.0921	1.1294	0.5029	0.0139	0.0500	0.0000	0.1039	99.3517
HW_67_2C.7	0.0494	97.8502	0.4507	0.0771	0.8494	0.4502	0.0161	0.0103	0.0114	0.0304	99.7952
HW_67_2C.8	0.0367	98.4435	0.3923	0.0793	0.4711	0.3600	0.0281	0.0055	0.0146	0.0055	99.8366
HW_67_2A.1	0.0207	98.1392	0.3500	0.0394	0.2971	0.4046	0.0230	0.0092	0.0000	0.0000	99.2832
HW_67_2A.2	0.0168	98.6566	0.3251	0.0947	0.2232	0.3480	0.0164	0.0061	0.0000	0.0137	99.7006
HW_67_2A.3	0.0299	98.1544	0.3769	0.0377	0.4877	0.4007	0.0068	0.0050	0.0000	0.0046	99.5037
HW_67_2A.4	0.0368	98.3526	0.3903	0.0367	0.5286	0.3913	0.0084	0.0000	0.0000	0.0119	99.7566
HW_67_2A.5	0.0213	97.9735	0.3903	0.0396	0.4417	0.3825	0.0070	0.0565	0.0000	0.0073	99.3197
HW_67_2A.6	0.0243	97.9694	0.3810	0.0331	0.5598	0.4369	0.0168	0.0014	0.0000	0.0000	99.4227
HW_67_2A.7	0.0282	97.4196	0.4063	0.0435	0.5689	0.4824	0.0192	0.0316	0.0000	0.0000	98.9997
HW_67_2A.8	0.0333	97.3902	0.3698	0.0366	0.6361	0.5919	0.0387	0.0032	0.0012	0.0097	99.1107
HW_67_2B.core1	0.0309	97.8754	0.3674	0.0353	0.6431	0.4526	0.0113	0.0144	0.0000	0.0000	99.4304
HW_67_2B.core2	0.0383	97.8671	0.3802	0.0419	0.7904	0.4807	0.0152	0.0275	0.0000	0.0396	99.6809
HW_67_2B.rim1	0.0356	98.0054	0.3551	0.0357	0.6303	0.5319	0.0291	0.0159	0.0070	0.0000	99.6460
HW_67_2B.rim2	0.0284	97.8031	0.3579	0.0617	0.4362	0.5615	0.0494	0.0195	0.0092	0.0000	99.3269
HW_50_3.1	0.0472	90.5638	0.3679	0.6972	2.8800	3.3334	0.7988	0.0418	0.0944	0.4980	99.3225
HW_50_3.2	0.0403	70.5046	0.2808	5.4168	2.2263	9.4281	7.1595	0.0278	0.5383	0.4471	96.0696
HW_50_4A.1	0.0176	27.9018	0.1100	15.9836	0.7444	26.4065	23.9194	0.0000	1.6775	0.0031	96.7639
HW_50_4A.2	0.0500	59.6505	0.2457	7.9539	1.7186	13.2224	10.3310	0.0352	0.8188	0.1313	94.1574
HW_50_4B.1	0.0586	86.1894	0.3126	1.8450	1.7025	4.9095	2.6670	0.0017	0.2510	0.1149	98.0522
HW_50_4B.2	0.0403	51.0683	0.1691	9.9188	1.0412	18.0407	16.2155	0.0000	1.1765	0.0371	97.7075

EPMA UNCERTAINTY

	ZrO2	TiO2	V2O3	Al2O3	Nb2O5	FeO	SiO2	Cr2O3	MnO	Ta2O5
FW_69_1.1	13.3	0.2	2.4	9.1	3.3	3.2	7.4	106.9	100.0	100.0
FW_69_2.1	8.4	0.2	2.4	6.7	3.0	2.6	5.9	1913.7	100.0	100.0
FW_69_3.1	14.2	0.2	2.3	6.4	4.6	3.0	5.7	154.4	100.0	100.0
FW_69_3.2	15.9	0.2	2.3	5.9	4.3	2.9	5.0	101.9	50.3	90.6
FW_69_3.3	16.7	0.2	2.6	6.5	5.7	3.0	6.5	62.9	145.1	217.3
FW_69_4.1	6.1	0.2	2.1	9.3	1.2	1.5	27.4	15.0	100.0	100.0
FW_69_4.2	6.9	0.2	2.3	10.1	1.4	1.6	172.1	16.2	100.0	13.6
FW_69_4.3	6.4	0.2	2.2	9.8	1.3	1.6	32.9	16.1	100.0	55.0
FW_69_4.4	6.1	0.2	2.1	8.5	1.3	1.8	33.6	16.1	69.5	55.8
FW_69_4.5	6.4	0.2	2.1	9.1	1.2	1.6	100.0	12.1	251.4	41.6
FW_69_4.6	6.2	0.2	2.1	9.5	1.3	1.6	32.5	16.4	100.0	8.4
FW_69_4.7	6.1	0.2	2.0	11.5	1.3	1.6	22.5	19.1	58.9	9.6
FW_68_1A.1	100.0	0.2	2.5	3.5	1.0	1.0	10.9	100.0	288.4	10.8
FW_68_1A.2	114.0	0.2	2.6	7.6	1.0	1.0	100.0	100.0	100.0	10.5
FW_68_1A.3	30.4	0.2	2.5	7.7	1.1	1.0	100.0	100.0	104.8	11.0
FW_68_1A.4	96.4	0.2	2.4	7.5	1.1	1.0	100.0	49.5	270.5	9.4
FW_68_1A.5	58.0	0.2	2.4	7.5	1.1	1.0	64.3	100.0	216.0	11.4
FW_68_1B.1	100.0	0.2	2.6	5.5	1.1	1.0	100.0	100.0	100.0	9.7
FW_68_1B.2	100.0	0.2	2.7	6.4	1.1	1.0	100.0	319.4	761.8	11.1
FW_68_4.1	5.9	0.2	2.7	9.2	1.9	0.9	11.4	100.0	18.2	58.4
FW_68_4.2	5.7	0.2	2.5	9.9	1.9	0.9	17.2	173.9	25.7	85.2
FW_68_2.1	14.6	0.2	2.7	14.9	1.1	0.5	14.0	654.1	4.2	53.1
FW_68_2.2	16.1	0.2	2.6	2.7	1.8	1.1	20.3	100.0	33.6	71.6
FW_68_2.3	14.8	0.2	2.8	12.1	2.0	1.1	34.0	100.0	155.3	101.1
FW_68_2.4	13.2	0.2	2.9	13.0	2.0	1.1	18.9	100.0	100.0	55.1
FW_68_2.5	14.8	0.2	2.7	15.1	1.9	1.1	17.1	100.0	277.5	232.6
FW_68_3.1	11.9	0.2	2.7	9.7	2.1	1.2	12.5	100.0	296.7	1623.4
FW_68_3.2	19.9	0.2	2.8	12.6	2.6	1.3	13.8	100.0	100.0	18436.0
FW_68_3.3	13.1	0.2	2.8	14.9	2.4	1.2	15.9	100.0	100.0	281.5
HW_50_1.1	100.0	0.3	2.7	15.2	1.1	1.0	100.0	35.8	88.8	13.8
HW_50_1.2	100.0	0.2	2.5	13.0	1.0	1.0	100.0	26.7	5549.0	10.2
HW_50_1.3	100.0	0.6	10.3	6.3	4.0	3.1	100.0	100.0	44.5	100.0
HW_50_1.4	100.0	0.6	10.4	18.7	3.8	2.8	100.0	100.0	17.4	100.0
HW_50_2.1	100.0	0.2	2.9	0.4	4.7	0.6	0.5	100.0	14.2	282.1
HW_50_2.2	20.5	0.2	2.9	0.7	2.2	1.0	0.7	76.2	20.6	25.8
HW_50_2.3	100.0	0.2	2.7	0.4	2.5	0.9	0.5	487.2	5.0	47.7
HW_50_2.4	11.6	0.2	2.6	3.5	2.2	0.9	4.3	40.0	35.3	47.7
HW_67_1.1	4.4	0.2	2.4	5.1	1.6	1.9	2.1	13.0	336.6	16.1
HW_67_1.2	4.1	0.2	2.3	5.7	1.5	1.8	6.6	10.0	100.0	11.3
HW_67_1.3	4.6	0.2	2.2	6.2	1.5	1.8	7.8	13.5	100.0	17.4
HW_67_1.4	4.8	0.2	2.4	5.3	1.5	1.8	14.3	12.7	107.8	18.0
HW_67_1.5	5.2	0.2	2.3	5.4	1.6	1.8	14.2	11.2	313.0	11.8
HW_67_1.6	4.7	0.2	2.3	5.4	1.6	1.7	12.6	17.1	55.0	13.4
HW_67_1.7	4.4	0.2	2.2	5.8	1.5	1.7	10.6	15.1	166.5	16.6
HW_67_1.8	4.6	0.2	2.2	5.2	1.6	1.8	5.6	14.6	100.0	15.4
HW_67_2C.1	14.0	0.2	2.5	15.2	5.9	2.0	12.5	51.4	100.0	100.0
HW_67_2C.2	5.1	0.2	2.4	12.1	2.2	2.0	29.4	47.1	100.0	28.8
HW_67_2C.3	4.8	0.2	2.3	10.6	1.9	2.0	25.2	21.7	100.0	22.9
HW_67_2C.4	4.4	0.2	2.2	6.0	1.8	1.8	199.4	23.2	100.0	12.1
HW_67_2C.5	4.4	0.2	2.2	5.9	1.8	1.8	51.0	29.8	98.2	13.7
HW_67_2C.6	4.4	0.2	2.2	5.4	1.7	2.1	35.5	24.6	100.0	16.3
HW_67_2C.7	4.9	0.2	2.3	6.5	2.3	2.2	31.1	121.6	74.3	54.2
HW_67_2C.8	6.5	0.2	2.5	6.2	3.8	2.7	18.1	223.1	56.8	300.2
HW_67_2A.1	11.2	0.2	2.6	11.8	5.7	2.4	21.7	133.4	100.0	100.0
HW_67_2A.2	13.5	0.2	2.7	5.3	7.8	2.7	30.5	201.4	100.0	117.8
HW_67_2A.3	7.9	0.2	2.5	12.5	3.7	2.4	73.7	245.5	100.0	354.3
HW_67_2A.4	6.5	0.2	2.4	12.8	3.5	2.5	57.3	100.0	100.0	138.5
HW_67_2A.5	10.9	0.2	2.4	11.7	3.9	2.6	71.7	19.7	100.0	227.2
HW_67_2A.6	9.7	0.2	2.5	14.2	3.0	2.3	29.4	911.9	100.0	100.0
HW_67_2A.7	8.3	0.2	2.4	10.8	3.2	2.2	25.9	38.8	100.0	100.0
HW_67_2A.8	7.1	0.2	2.6	13.0	2.9	1.9	13.1	388.9	721.1	172.2
HW_67_2B.core1	7.6	0.2	2.6	13.2	2.9	2.3	44.3	84.9	100.0	100.0
HW_67_2B.core2	6.3	0.2	2.5	11.3	2.4	2.2	33.1	44.7	100.0	41.3
HW_67_2B.rim1	6.7	0.2	2.6	13.3	2.9	2.0	17.4	77.4	120.6	100.0
HW_67_2B.rim2	8.3	0.2	2.6	7.8	4.1	1.9	10.4	63.3	93.7	100.0
HW_50_3.1	5.2	0.2	2.6	1.1	0.9	0.6	1.0	29.8	10.2	3.7
HW_50_3.2	6.3	0.3	3.1	0.3	1.1	0.3	0.3	43.6	2.2	3.9
HW_50_4A.1	14.8	0.4	6.6	0.2	2.8	0.2	0.2	100.0	1.0	530.4
HW_50_4A.2	5.1	0.3	3.5	0.3	1.3	0.3	0.2	33.7	1.6	12.6
HW_50_4B.1	4.3	0.2	2.8	0.6	1.3	0.5	0.5	721.0	4.1	14.6
HW_50_4B.2	6.5	0.3	4.5	0.2	2.1	0.2	0.2	100.0	1.3	44.2

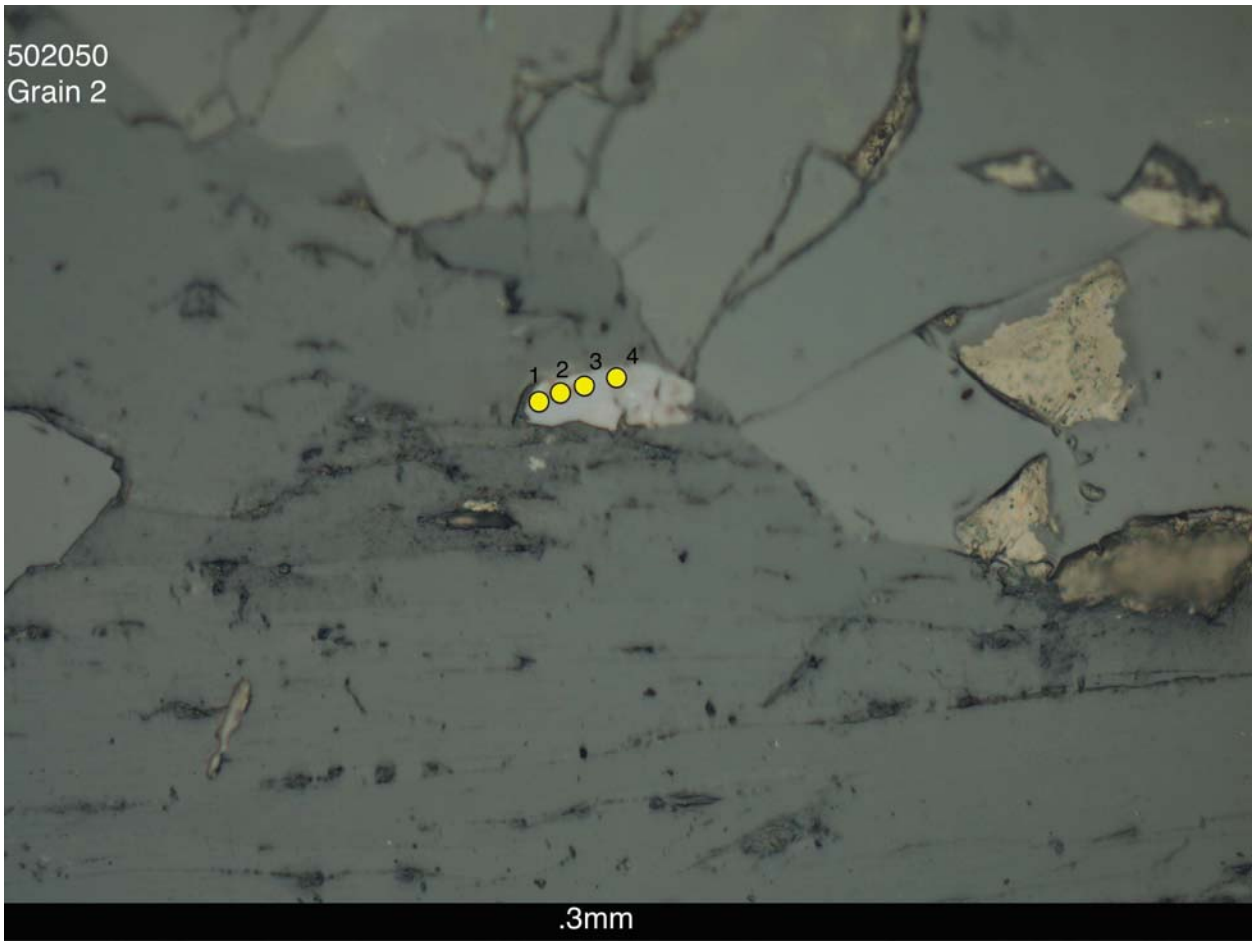
502050
Grain 2
1
2
3
4
.3mm

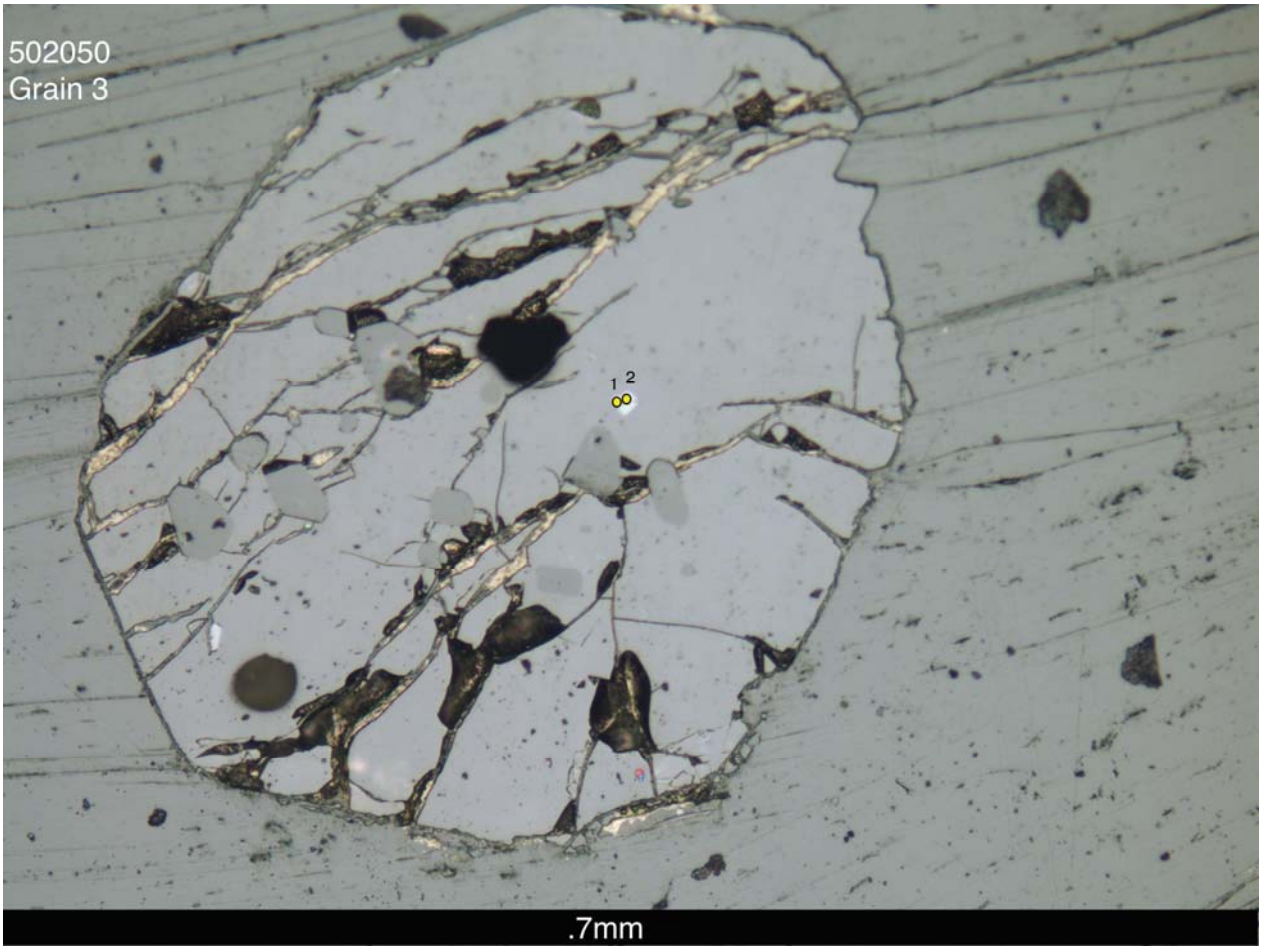
502050
Grain 3
1
2
.7mm

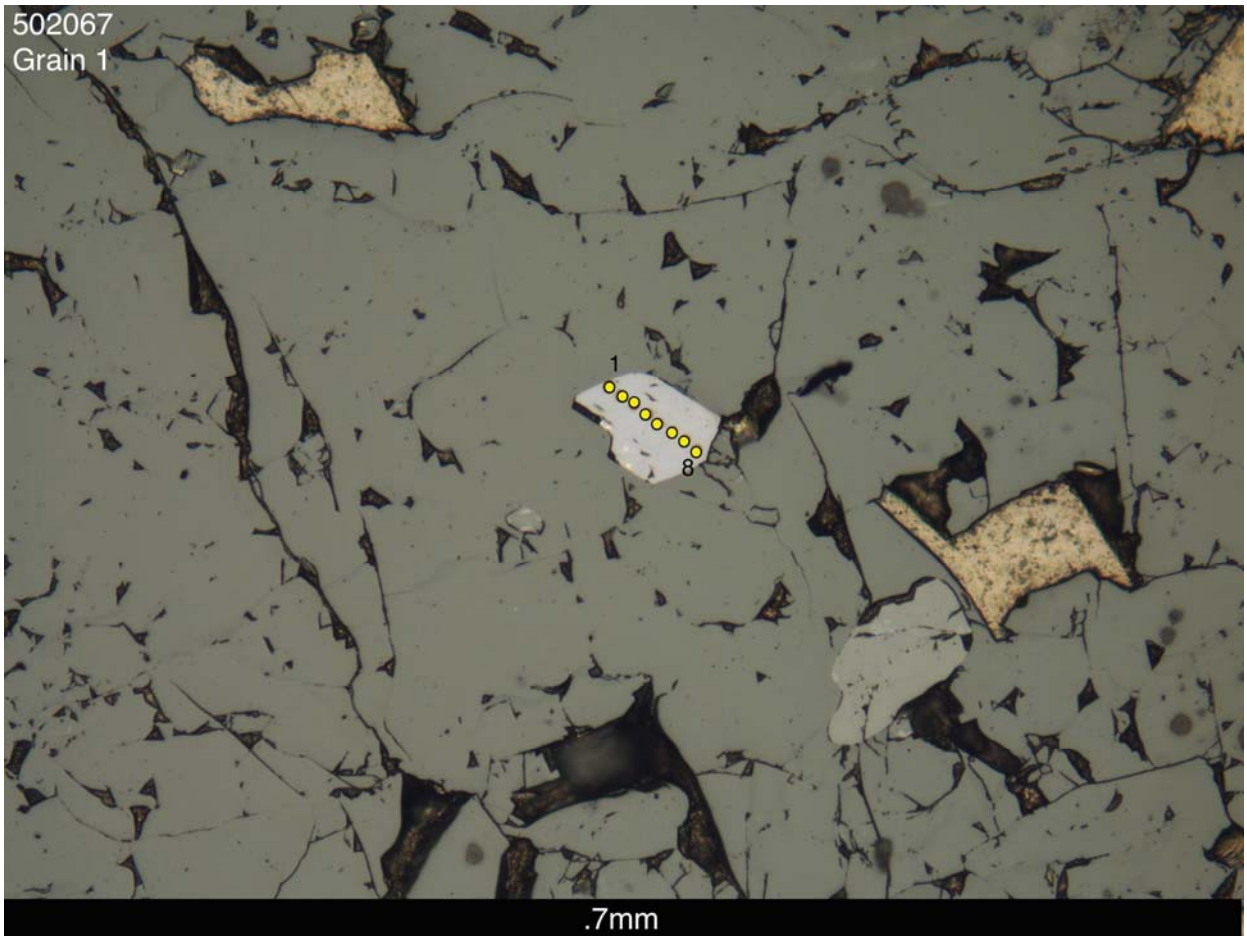
502067
Grain 1
1
8
.7mm

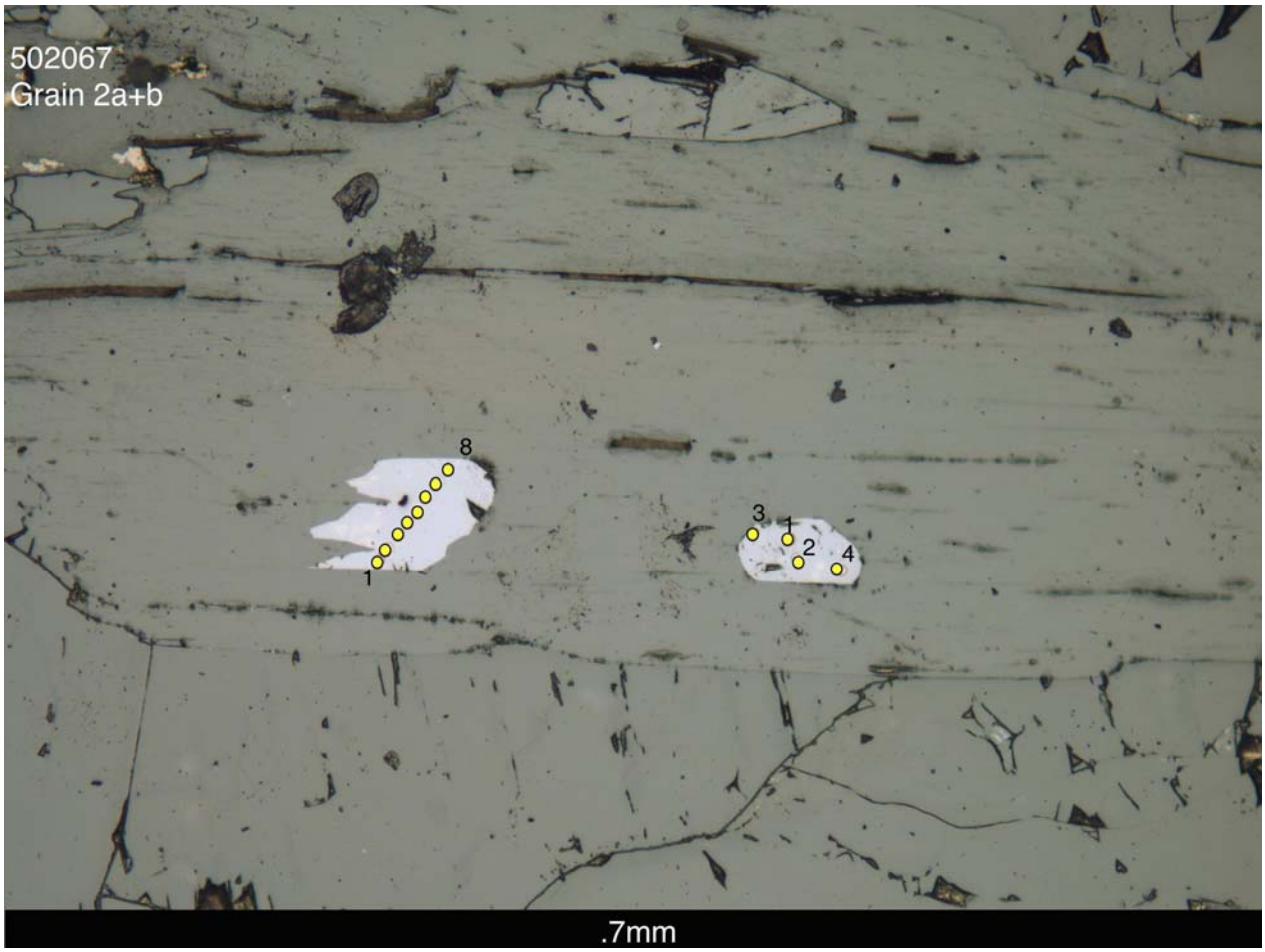
502067
Grain 2a+b
8
1
3
1
2
4
.7mm

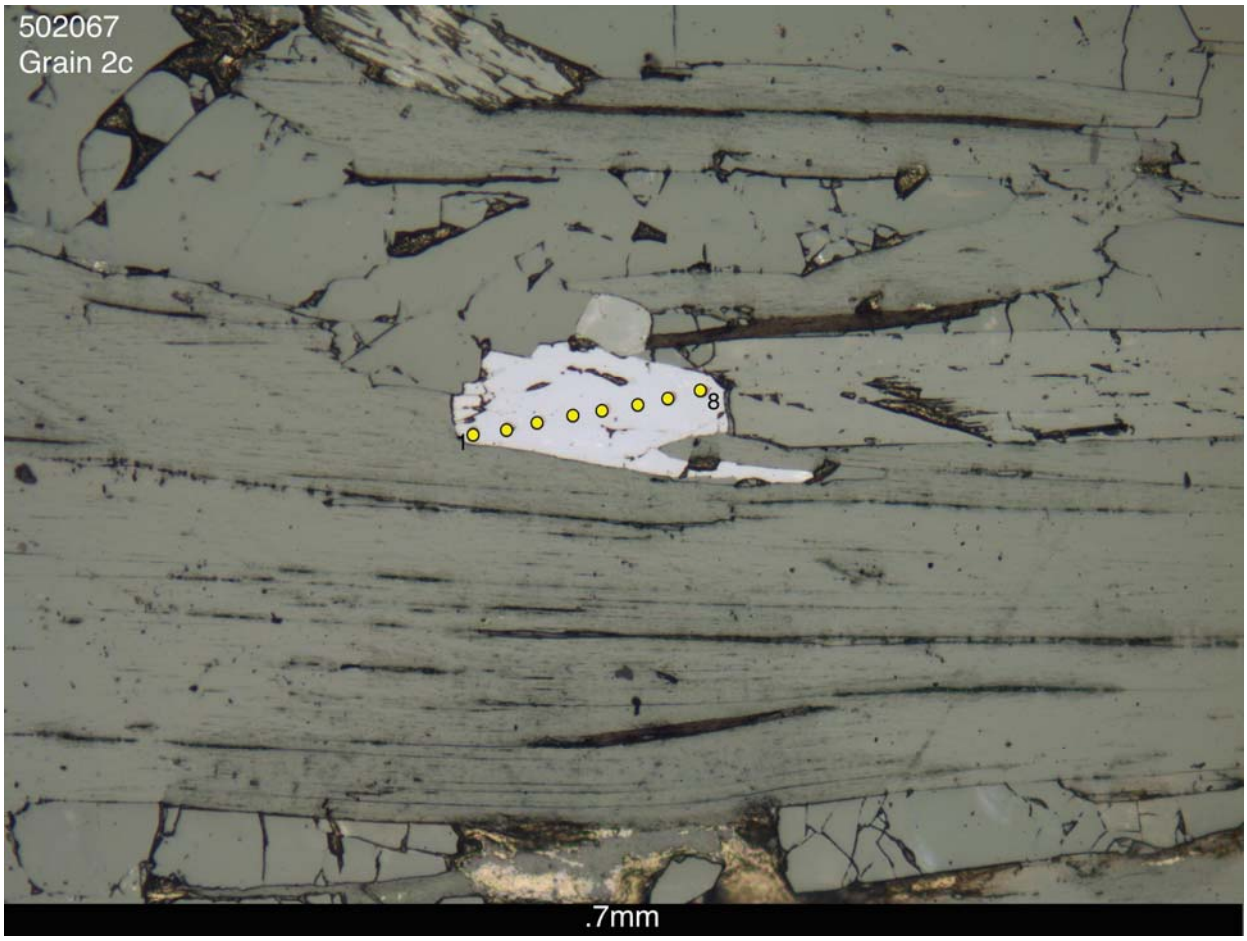
502067
Grain 2c
1
8
.7mm

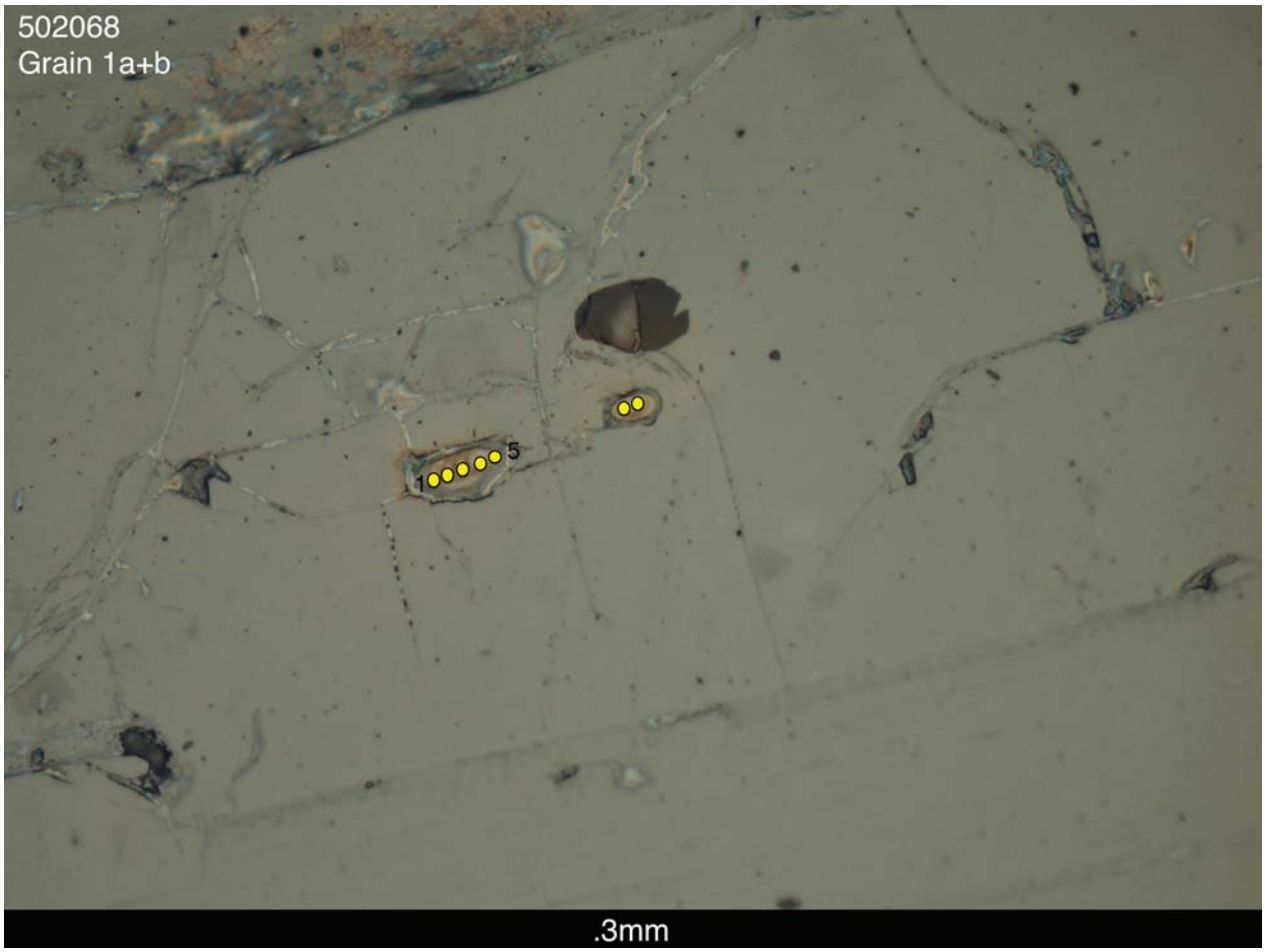
502068
Grain 1a+b
1
5
.3mm

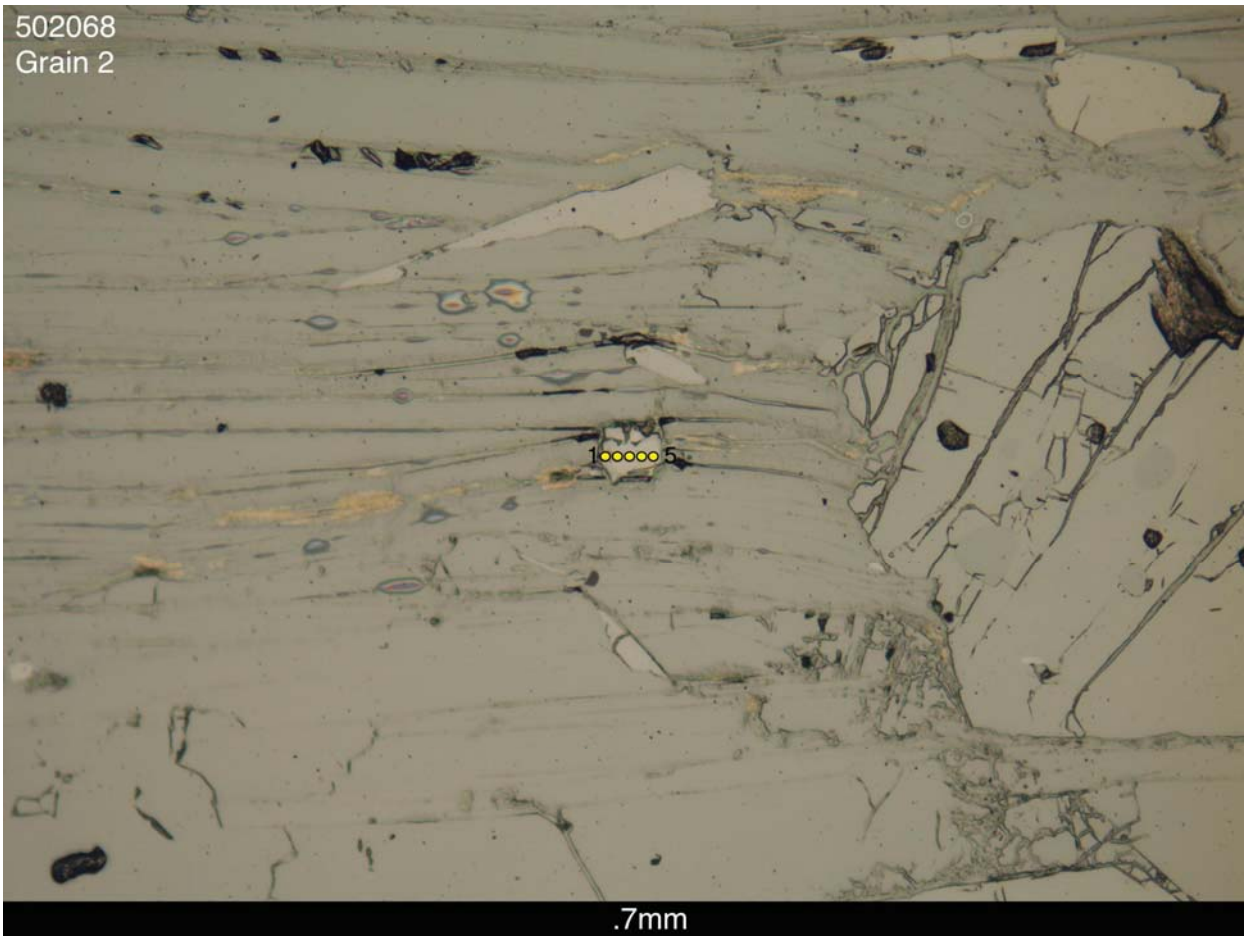
502068
Grain 2
1
5
.7mm

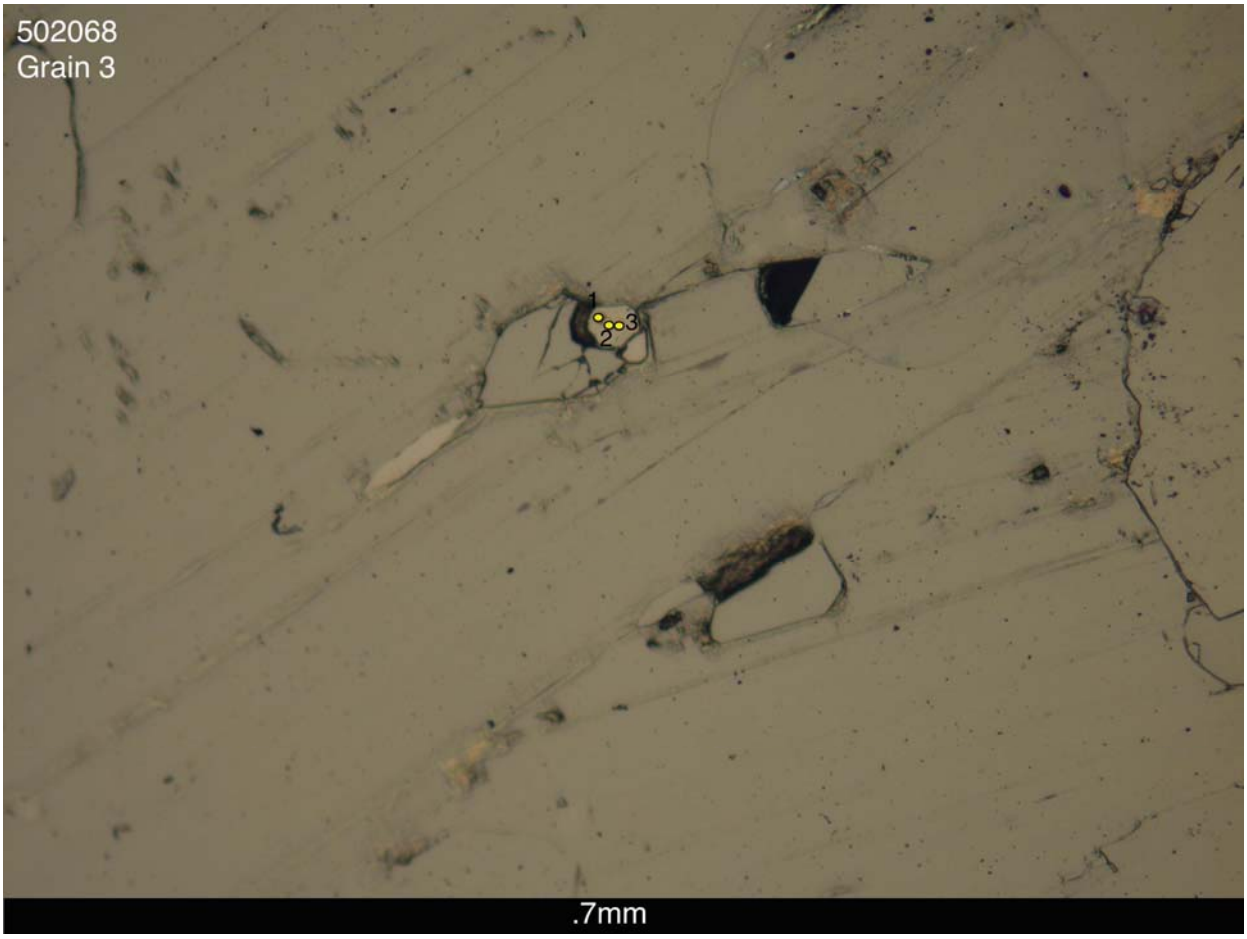
502068
Grain 3
1
2
3
.7mm

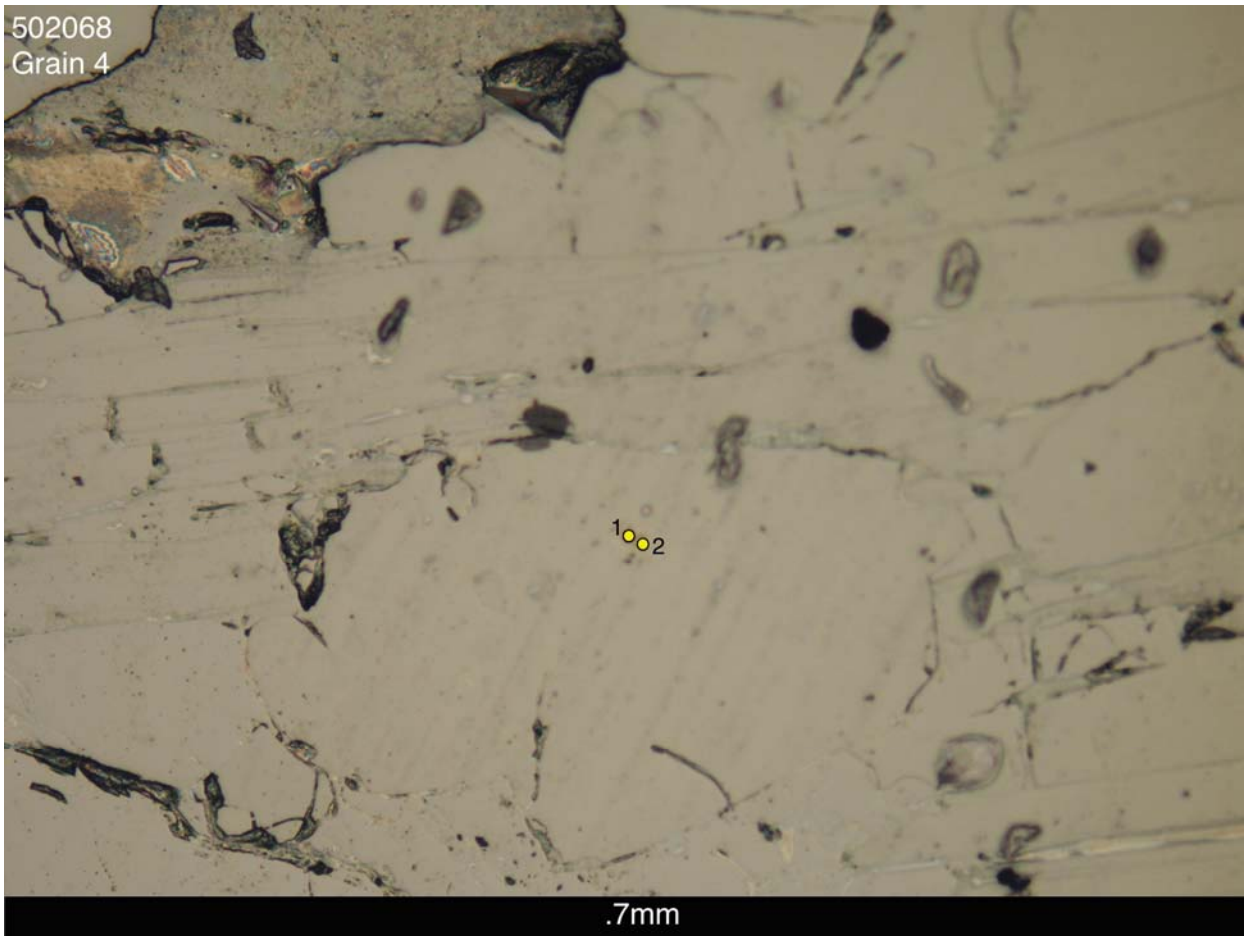
502068
Grain 4
1
2
.7mm

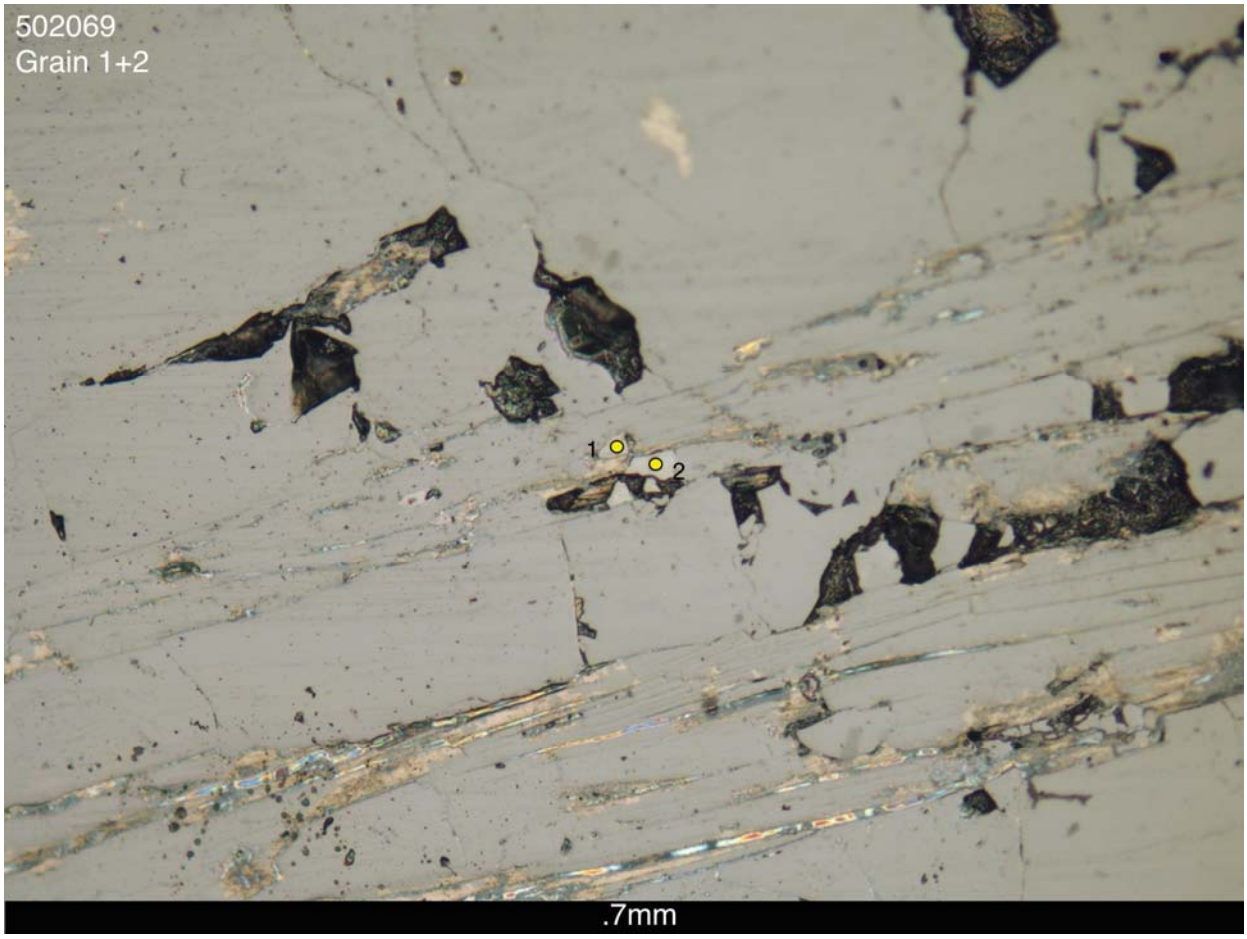
502069
Grain 1+2
1
2
.7mm

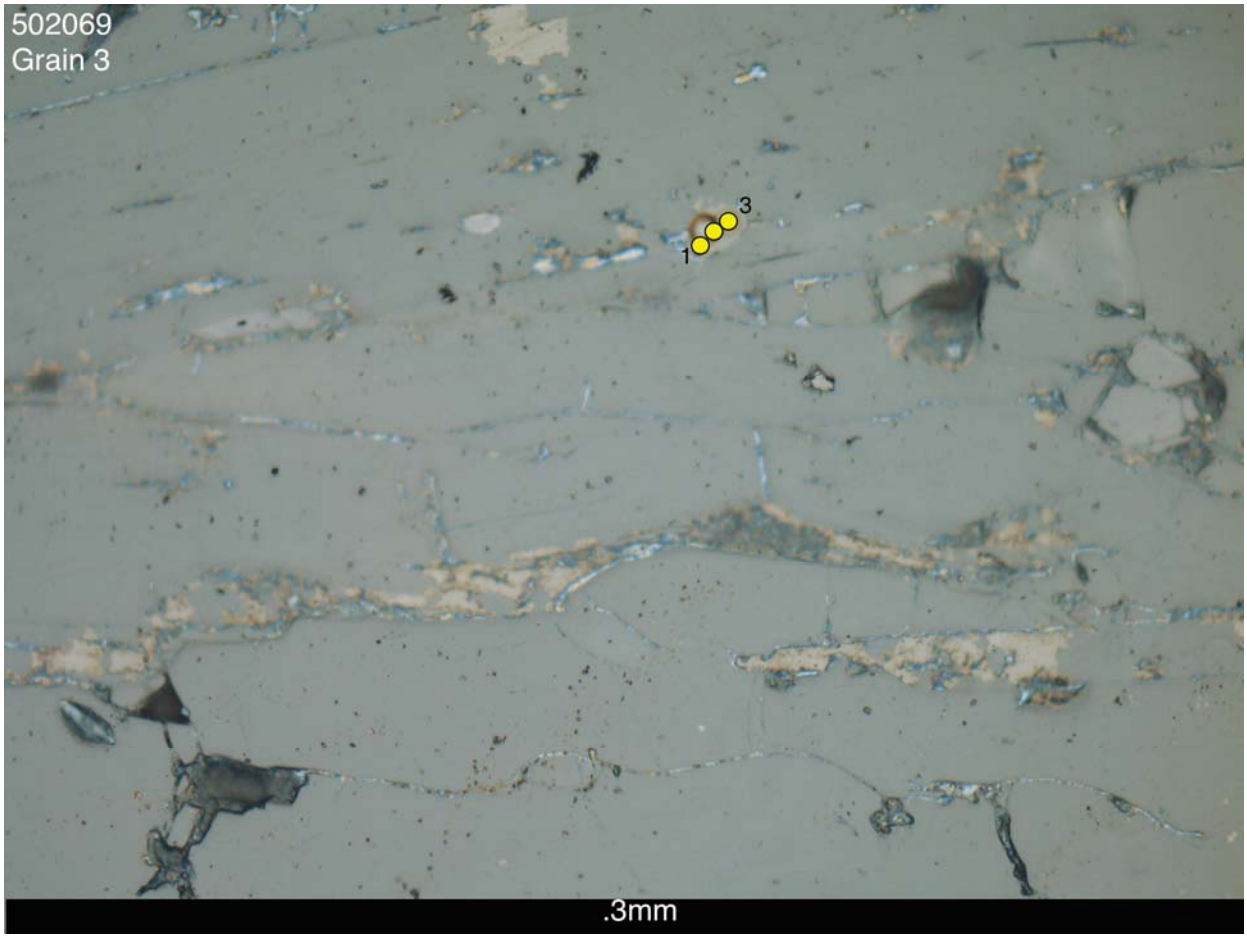
502069
Grain 3
1
3
.3mm


502069
Grain 4
1
2
3
4
5
6
7
.7mm